Spin susceptibilities of altermagnets

Author
William Skoglund

Supervisor
Erik van Loon

Thesis submitted for the degree Bachelor of Theoretical Physics
Project duration: II Months

LUND
UNIVERSITY

Department of Physics
Division of Mathematical Physics
May 2024

Acknowledgements

I was very fortunate to have Erik as my supervisor for this project. His hospitality, insightful comments and availability for questions were tremendously appreciated. Our weekly meetings were of great importance for understanding concepts on a deeper level and setting clear goals. I am thankful for him finding such an interesting thesis project, and I am eager to continue working with him in condensed matter physics. This project would certainly not have been possible without his great help and expertise.

Furthermore, I would like to thank my mother Åsa, father Mats, brother Oliver, grandmother Monica and grandfather Arne for their unwavering support throughout my upbringing, especially during my bachelor's degree. I am very lucky to have such a supportive family. Lastly, I would like to thank my closest friends and dearly beloved ones, Emma, Jakob and most importantly Wilma, for always being present and cheering me on.

Abstract

Altermagnetism is an emerging field within condensed matter physics. This new magnetic phase has been theoretically considered and later experimentally observed. The combination of no net magnetization and a spin dependent electronic band structure make altermagnets appealing candidates for applications within fields such as spintronics and superconductivity. Through numerical considerations, the spin-flip susceptibilities of altermagnets are predicted to show a splitting in $(\omega, \vec{q})$-space, which is not displayed by antiferromagnets. Using inelastic neutron spectroscopy to probe for this splitting has been suggested as an experimental procedure to detect altermagnetic materials. In this thesis, we analytically study spin susceptibilities of a simple minimal model for a non-interacting altermagnetic electron gas. Expressions for the imaginary part of various spin susceptibilities are obtained, and subsequently verified by numerical considerations and comparisons with known limiting cases. Then, single-particle excitation spectra associated with the considered susceptibilities are discussed. Finally, further analytical considerations, such as accounting for electron-electron interactions, are suggested.

Contents

1 Introduction

At the end of the 19th century, modern models describing magnetic phenomena in solids were beginning to be developed. In 1907, Pierre Weiss suggested that the magnetic behaviour associated with a strong response to an external magnetic field, known as ferromagnetism, originates from a strong molecular magnetic field, acting on localized atomic magnetic moments[1]. This magnetic field would, provided a sufficiently low temperature, cause the moments to align in parallel.

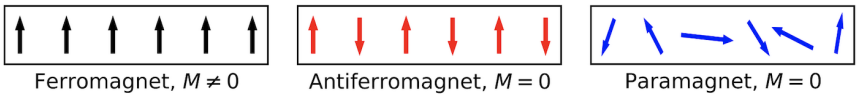

Figure 1: Alignment of localized atomic magnetic moments at low temperatures and in the absence of an external magnetic field. The observed magnetization is M.

The long-range alignment of moments would lead to a spontaneous magnetization in the absence of an external magnetic field, which is depicted in the leftmost panel of Fig.1. Furthermore, Weiss postulated that ferromagnetic solids are composed of many regions, known as domains, where moments are locally aligned in parallel[1]. This would explain why certain ferromagnetic materials do not exhibit a spontaneous magnetization below the critical temperature, as the moments are aligned inside of the domains, but the overall contribution cancels out.

Ferromagnets could be classically modelled using the Ising model[2], introduced in 1920. Specifically, the Ising model considers localized moments in a lattice arrangement, akin to that depicted in Fig.1. The moments are modelled as having short-ranged interactions which promote the alignment of neighbouring moments. This model was able to predict the spontaneous magnetization of ferromagnets below some critical temperature. In 1928, the Ising model was re-formulated in terms of quantum mechanics by Werner Heisenberg[1]. This allowed Heisenberg to identify the interaction tending to align neighbouring moments, called the exchange interaction, as being of quantum mechanical origin.

Inspired by the work of Heisenberg and Weiss, Louis Néel would in 1932 consider a new magnetic phase known as antiferromagnetism. This magnetic phase would be characterized by adjacent moments aligning in an anti-parallel configuration, leading to no macroscopic magnetization. Lev Landau would, during the same period as Néel, independently develop a theory for antiferromagnetism to account for anomalies in experimental measurements of magnetic susceptibilities. Landau was also able to show that domain formation in ferromagnetic materials, as postulated by Weiss, would indeed minimize the total energy[1]. Shortly after Neél's theoretical prediction, antiferromagnetism was experimentally confirmed, which resulted in Neél being awarded the Nobel prize in 1970[3].

[1]For future reference, "localized moments", or "moments" will refer to localized atomic magnetic moments.

Understanding the origin and physical properties of different magnetic phases is an area of interest in modern solid state physics. It is now understood that magnetic effects of appreciable size are indeed associated with long-range ordering of moments in solids. As mentioned, this is the origin of ferromagnetism and antiferromagnetism. Unlike the aforementioned magnetic phases, paramagnetism is a magnetic phase associated with ordering of moments only in the presence of an external magnetic field. The orientation of moments for the discussed magnetic phases are depicted in Fig.1.

The lattice structure and magnetic profile of a metal determines the energy of itinerant electrons through the dispersion relation, also known as the electronic band structure. Ferromagnets display a spin-dependent dispersion relation, but this is not the case for antiferromagnets [4].

Recently, a new magnetic phase called altermagnetism was theoretically predicted, and later experimentally observed[5]. Altermagnets display a spin-dependent dispersion relation and an anti-parallel magnetic moment ordering, meaning they have no net magnetization. That is, altermagnets share features with both ferromagnets, and antiferromagnets.

Altermagnets are suggested to have many interesting applications. For instance, the spin-split electronic band structure and the net zero magnetization is expected to contribute greatly to the field of spintronics[4], which aims at utilizing the intrinsic spin of electrons along with their electrical transport properties to enhance the effectiveness of electrical devices[6]. Moreover, altermagnets have been considered in the context of unconventional superconductivity, attributed to their net zero magnetization and spin-split dispersion relation. Superconductivity would then be obtained through a different pathway than what is usually expected, as the spin-splitting makes conventional superconductivity less energetically favourable[4][7].

Numerical considerations have shown a variety of interesting physical properties of altermagnets, such as the imaginary part of the spin-flip susceptibilities being chirality dependent[8], which is not the case for antiferromagnets. This chirality dependence causes the spin-flip susceptibilities to be split in $(\omega, \vec{q})$-space. This splitting could be observed using inelastic neutron spectroscopy of sufficient resolution[9]. As such, it has been suggested as a probe to test materials for altermagnetic behaviour[8]. Advanced neutron facilities such as the European Spallation Source (ESS) in Lund are planning on making inelastic neutron spectroscopy of high-energy resolution available to study spin dynamics[10]. Such facilities could then be used to test various materials for altermagnetism.

The aim of this thesis is to analytically determine various spin susceptibilities of a simple minimal model of a non-interacting altermagnetic electron gas.

2 Theory

2.1 Magnetic phases and altermagnets

Magnetic phases are categorized by their associated symmetries, which define their physical properties. Paramagnets display spin-flip symmetry, ferromagnets are symmetric under translation and antiferromagnets are symmetric under combined spin-flip and translation. Of the mentioned phases, only the ferromagnetic phase displays a non-zero magnetization, or

$$M = \sum_{\sigma} \int d\vec{k}\ \sigma n_{\vec{k}\sigma}, \tag{2.1}$$

is non-zero for sufficiently low temperatures. In Eq. (2.1), σ denotes spin $(\uparrow, \downarrow)$, and $n_{\vec{k}\sigma}$ is the particle density.

Altermagnetism has recently been theoretically considered as a new magnetic phase, and later experimentally confirmed[4][5]. This magnetic phase is characterized by its particular anti-parallel magnetic ordering, leading to no net magnetization and $\mathcal{PT}$ (parity times time-reversal) symmetry breaking. Furthermore, the $\mathcal{PT}$ symmetry breaking causes the dispersion relation to become spin-dependent[8]. Structurally, altermagnets consist of two opposite spin sub-lattices connected by a discrete rotation, making them associated with a combined spin-flip and rotation symmetry. This is displayed in Fig. 2.

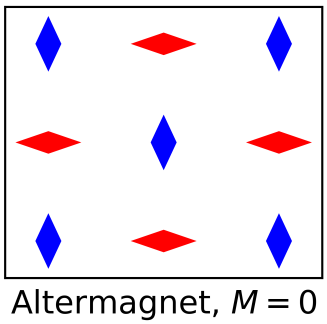

Figure 2: Lattice model of altermagnets, displaying a combined spin-flip and rotation symmetry. The color of the lattice sites denote their associated spin, and the rhombus shape of the lattice sites are used to depict rotation symmetry.

To model the altermagnetic phase, we must choose an appropriate dispersion relation, respecting the aforementioned symmetry requirements. In general, the dispersion relation depends on the potential generated by the lattice structure, and the magnetic type of the metal. Dispersion relations for real metals are complicated, but they can be approximated around a minimum according to[2] $\varepsilon(\vec{k}, \sigma) = \frac{\vec{k}^2}{2m}$, where $\vec{k}$ is the wave vector of the electron's

[2]We will take $\hbar = 1$ throughout this thesis.

wave function, and m is the effective electron mass. The effective mass of itinerant electrons depends on the potential generated by the lattice structure. That is, the effective mass tensor accounts for lattice interactions. More generally, if there is no spin-orbit coupling then the dispersion relation of a d-dimensional solid can be approximated around a minimum as

$$\varepsilon(\vec{k},\sigma) = \frac{1}{2}\sum_{i,j=1}^{d} [\mathcal{M}^{\sigma}{}_{ij}]^{-1}\, k_i k_j, \text{ where } [\mathcal{M}^{\sigma}{}_{ij}]^{-1} = \frac{\partial^2 \varepsilon}{\partial k_i \partial k_j} \text{ is the inverted effective mass tensor.}$$

Mathematically, the effective mass tensor depends on the curvature of the dispersion relation. Note that $\mathcal{M}^{\sigma}{}_{ij}$ can always be diagonalized by an appropriate choice of coordinates.

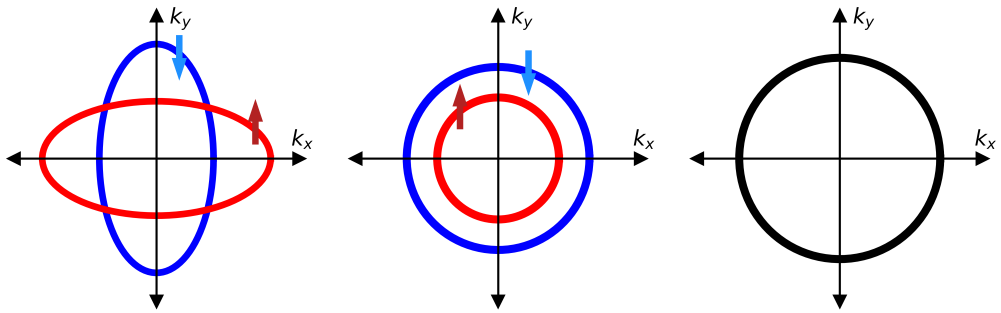

Figure 3: From left to right, examples of Fermi surfaces of an altermagnet, ferromagnet and antiferromagnet. The altermagnet and ferromagnet have spin-split Fermi surfaces. The blue curve represents the Fermi surface for spin down electrons, and the red curve represents the Fermi surface for spin up electrons.

Based on electronic band structures obtained from Hamiltonians modelling the altermagnetic phase[4], a simple model for the dispersion relation of a two dimensional non-interacting altermagnetic electron gas could be constructed by two spin dependent hyperbolas in $\vec{k}$-space, connected by a 90° degree rotation. The effective mass tensors of the two hyperbolas would have to be related through the exchange of the diagonal matrix elements, in order for the dispersion relation to have a spin-flip and 90° rotation symmetry[3]. Mathematically, such a dispersion relation can be modelled as

$$\varepsilon(\sigma,\vec{k}) = \delta_{\sigma\uparrow}\left(\frac{k_x^2}{2m_1} + \frac{k_y^2}{2m_2}\right) + \delta_{\sigma\downarrow}\left(\frac{k_y^2}{2m_1} + \frac{k_x^2}{2m_2}\right). \tag{2.2}$$

Here $\vec{k}$ is the two dimensional wave vector of the electron's wave function, and σ is the electron's spin ($\uparrow$ or $\downarrow$). Constant energy surfaces of such a dispersion relation would consist of two spin-dependent ellipses connected by a 90° rotation. This is displayed in Fig. 3.

[3]See Sec. 6.1 in the appendix for the proof of this statement for the suggested dispersion relation.

For all calculations in this thesis, we will consider two-dimensional magnetic phases at zero temperature. Furthermore, we will assume that the considered magnetic system displays translational symmetry, and that no spin-orbit coupling is present. This means the wave vector of the electron's wave function, $\vec{k}$, and electron's spin, σ, are both good quantum numbers. We will assume the Hamiltonian describing our system to be time-independent, and that no electron-electron interactions are occurring. However, as mentioned, interactions are accounted for by the effective mass tensor.

2.2 Linear response theory

Linear response theory considers the problem of determining the change in the average of a physical quantity when a weak perturbation slightly displaces a system from thermal equilibrium. For a sufficiently weak perturbation, the change of the thermodynamic average can be approximated as being linearly dependent on the perturbing field. An essential quantity in calculating this change is the generalized susceptibility, defined in accordance to the notation in [11], as

$$\chi_{AB}(\vec{r},\vec{r'},t) \equiv -i\Theta(t)\left\langle\left[\hat{A}(\vec{r},t),\hat{B}(\vec{r'})\right]\right\rangle_0, \tag{2.3}$$

where $\hat{A}$ is the considered observable and $\hat{B}$ is an observable to which the time dependent perturbing field $F(t)$ couples to. That is, the perturbed Hamiltonian is formulated as $\hat{H}_F(t) = \hat{H}_0 + F(t)\hat{B}$. Furthermore, $\Theta(t)$ is the Heaviside step function[4]. The subscript 0 indicates the expectation value of the commutator is calculated with respect to the unperturbed Hamiltonian in thermal equilibrium. Note that the susceptibility χ_{AB} is a property of the equilibrium system.

For systems with translational symmetry, the Fourier transform of the susceptibility can be shown to depend on a single momentum $\vec{q}$ and some frequency ω. Specifically, the Fourier transform is in this case given by[5]

$$\chi_{AB}(\vec{q},\omega) = \lim_{\eta\to 0}\frac{1}{L^d}\int d\vec{r}e^{-i\vec{q}\cdot\vec{r}}\int d\vec{r'}e^{i\vec{q}\cdot\vec{r'}}\int_{-\infty}^{\infty}\chi_{AB}(\vec{r},\vec{r'},t)e^{i(\omega+i\eta)t}\,dt. \tag{2.4}$$

To ensure that the system was initially at equilibrium, we introduced a convergence factor $e^{-\eta t}$ to the temporal Fourier transform, where η is some small positive number. This corresponds to slowly turning on the perturbation. Once a final result is obtained, the limit $\eta \to 0$ is taken to obtain the physically relevant result. Physically, this corresponds to introducing damping to the system. The limit will be omitted for brevity.

Susceptibilities can be experimentally measured through spectroscopy. Specifically, correlations between electrons, describing the probabilistic relationship of finding two electrons at different positions at different times, can be measured using spectroscopy. Inelastic neutron spectroscopy is used to determine spin-spin correlation functions. Here, neutrons of

[4]The Heaviside step-function will be referred to as the "theta function" throughout the thesis.

[5]See Sec. 6.2 in the appendix for the derivation of this formula.

known spin polarization and well-defined momentum and energy are scattered off a material, coupling to spin densities inside of the material during the scattering event. The energy, momentum and spin polarization of outgoing neutrons are then measured, which allows for the determination of the momentum and energy transfer. Subsequently, the spin-spin correlation function is obtained, from which the spin susceptibility is derived from the fluctuation-dissipation theorem[12].

2.3 Linear response theory for independent electrons

Consider the creation and annihilation operators $\hat{c}^\dagger_\alpha$, $\hat{c}_\alpha$ for fermions, where $\hat{c}^\dagger_\alpha$ creates single-particle state $|\phi_\alpha\rangle$, and $\hat{c}_\alpha$ destroys it. Here, α denotes all good quantum numbers. Then, any one-particle operator $\hat{V}^{(1)}$, defined as consisting of a sum of N identical operators, each acting only on a specific electron, must be symmetric due to indistinguishably. This allows for the decomposition [11]

$$\hat{V}^{(1)} = \sum_{i=1}^{N} \hat{V}_i = \sum_{\alpha\beta} V_{\beta\alpha} \hat{c}^\dagger_\beta \hat{c}_\alpha. \tag{2.5}$$

The matrix element $V_{\beta\alpha}$ is given by

$$V_{\beta\alpha} \equiv \langle i, \beta | \hat{V}_i | i, \alpha \rangle = \sum_{s,t} \int d\vec{r}_i \, \phi^*_\beta(\vec{r}_i, t) [\hat{V}]_{t,s} \phi_\alpha(\vec{r}_i, s),$$

where index i denotes the ith electron, and the sum is over spins. We are able to express the susceptibility for single particle operators $\hat{A}$ and $\hat{B}$, acting on independent electrons in terms of the matrix elements of the operators, according to[6]

$$\chi^{(0)}_{AB}(\vec{q}, \omega) = \frac{1}{L^d} \sum_{\alpha\beta} \frac{n_\alpha - n_\beta}{\omega + \varepsilon_\alpha - \varepsilon_\beta + i\eta} \left(A_{\vec{q}}\right)_{\alpha\beta} \left(B_{-\vec{q}}\right)_{\beta\alpha}, \tag{2.6}$$

where $n_\alpha = \frac{1}{e^{\beta(\varepsilon_\alpha - \mu)} + 1}$ is the Fermi-Dirac distribution. The superscript (0) indicates that electron-electron interactions are not accounted for. We may express the imaginary part of Eq.(2.6) in the limit $\eta \to 0$ as

$$\mathrm{Im}\chi^{(0)}_{AB}(\vec{q}, \omega) = -\frac{\pi}{L^d} \sum_{\alpha\beta} (n_\alpha - n_\beta) \, \delta(\omega + \varepsilon_\alpha - \varepsilon_\beta) \left(A_{\vec{q}}\right)_{\alpha\beta} \left(B_{-\vec{q}}\right)_{\beta\alpha}. \tag{2.7}$$

The real part of the susceptibility may be obtained from its imaginary part, via Kramers-Kronig relations[11]. This means the physical implications of the susceptibility can be obtained from its imaginary part. Physically, Eq. (2.7) describes the sum over probabilities of exciting electrons from a region n_α with constant energy ε_α, to another region n_β of constant energy ε_β. The delta term in Eq. (2.7) reflects conservation of energy. The imaginary part of the Fourier transformed susceptibility, $\mathrm{Im}\chi^{(0)}_{AB}(\vec{q}, \omega)$, is related to the electron-hole excitation spectrum[11], where the magnitude of $\mathrm{Im}\chi^{(0)}_{AB}(\vec{q}, \omega)$ is related to the probability of an

[6] See Secs. 6.2 and 6.3 in the appendix for how Eq. (2.6) is obtained using results from [11].

electron-hole excitation occurring from the ground state. Specifically, an excitation where an electron absorbs energy ω and momentum $\vec{q}$ from some weak perturbation, resulting in its promotion to a new state, and the creation of a hole at the previously occupied electron state [13].

2.4 Spin density and second quantization

Using the spin-$\frac{1}{2}$ Pauli matrices, denoted as $\hat{\sigma}_\alpha$ for $\alpha = x, y, z$, we may define relevant spin operators as $\hat{S}_\alpha = \frac{1}{2}\hat{\sigma}_\alpha$ for $\alpha = x, y, z$. Furthermore, we define the spin-flip operators as $\hat{S}_\pm = \hat{S}_x \pm i\hat{S}_y$. The aforementioned spin operators act on the spin Hilbert space of a single, specific site in real space. These operators have second quantized representations, which are given by

$$\hat{S}_+ = \hat{c}^\dagger_\uparrow \hat{c}_\downarrow \ , \ \hat{S}_- = \hat{c}^\dagger_\downarrow \hat{c}_\uparrow \ , \ \hat{S}_x = \frac{1}{2}\left(\hat{c}^\dagger_\uparrow \hat{c}_\downarrow + \hat{c}^\dagger_\downarrow \hat{c}_\uparrow\right) \ , \ \hat{S}_y = \frac{1}{2i}\left(\hat{c}^\dagger_\uparrow \hat{c}_\downarrow - \hat{c}^\dagger_\downarrow \hat{c}_\uparrow\right) \ , \ \hat{S}_z = \frac{1}{2}\left(\hat{c}^\dagger_\uparrow \hat{c}_\uparrow - \hat{c}^\dagger_\downarrow \hat{c}_\downarrow\right),$$

according to Eq.(2.5). We then define spin density operators according to

$$\hat{\vec{S}}_\alpha(\vec{r}) = \sum_i \hat{\vec{S}}_{\alpha,i}\delta(\vec{r} - \hat{\vec{r}}_i), \tag{2.8}$$

where $\hat{\vec{S}}_{\alpha,i}$[7] is one of the aforementioned spin operators acting only on the spin Hilbert space of the ith site in real space, and $\hat{\vec{r}}_i$ is the position operator acting only on the spatial Hilbert space of the ith site in real space. It should be noted that $\hat{\vec{S}}_\pm(\vec{r})$ are not spin-density operators in the sense of measuring spin density. Instead, these operators act to flip the spins of the ith site in real space. The spatial Fourier transform of a spin-density operator is obtained as

$$\hat{S}_{\vec{q},\alpha} \equiv \hat{\vec{S}}_\alpha(\vec{q}) = \sum_i \hat{\vec{S}}_{\alpha,i} e^{-i\vec{q}\cdot\vec{r}_i}.$$

Note that spin density operators, and their Fourier transforms, are one-particle operators. Hence, they have second quantized representations given by[8]

$$\begin{aligned}
&\hat{S}_{\vec{q},+} = \sum_{\vec{k}} \hat{c}^\dagger_{\vec{k}-\vec{q}\uparrow}\hat{c}_{\vec{k}\downarrow} \ , \ \hat{S}_{\vec{q},-} = \sum_{\vec{k}} \hat{c}^\dagger_{\vec{k}-\vec{q}\downarrow}\hat{c}_{\vec{k}\uparrow} \ , \ \hat{S}_{\vec{q},z} = \frac{1}{2}\sum_{\vec{k}}\left(\hat{c}^\dagger_{\vec{k}-\vec{q}\uparrow}\hat{c}_{\vec{k}\uparrow} - \hat{c}^\dagger_{\vec{k}-\vec{q}\downarrow}\hat{c}_{\vec{k}\downarrow}\right), \\
&\hat{S}_{\vec{q},x} = \frac{1}{2}\sum_{\vec{k}}\left(\hat{c}^\dagger_{\vec{k}-\vec{q}\uparrow}\hat{c}_{\vec{k}\downarrow} + \hat{c}^\dagger_{\vec{k}-\vec{q}\downarrow}\hat{c}_{\vec{k}\uparrow}\right) \ , \ \hat{S}_{\vec{q},y} = \frac{1}{2i}\sum_{\vec{k}}\left(\hat{c}^\dagger_{\vec{k}-\vec{q}\uparrow}\hat{c}_{\vec{k}\downarrow} - \hat{c}^\dagger_{\vec{k}-\vec{q}\downarrow}\hat{c}_{\vec{k}\uparrow}\right).
\end{aligned} \tag{2.9}$$

2.5 Fourier transform of spin susceptibilities

To obtain the susceptibilities for the modelled altermagnetic state, we must specify which quantum numbers commute with its Hamiltonian. Since we are assuming translational symmetry and no spin-orbit coupling, the wave vector $\vec{k}$ and spin σ are good quantum numbers.

[7] The notation of spin operators follows that from [11].

[8] These expressions are derived in Sec. 6.5 in the appendix.

Then, we use the single particle eigenstates $\alpha = |\vec{k}\sigma\rangle$ as a basis for the single-particle Hilbert space. The wave function can be realized by $\phi_{\vec{k}\sigma}(\vec{r}, s) = \frac{1}{\sqrt{L^d}} e^{i\vec{k}\cdot\vec{r}}\delta_{s\sigma}$, where $\vec{r}$ is the position, and s is the spin of the electron. The constant $1/\sqrt{L^d}$ is a normalization factor. By Eq.(2.6), the general susceptibility modelling our non-interacting altermagnetic electron gas is given by

$$\chi^{(0)}_{AB}(\vec{q}, \omega) = \frac{1}{L^d} \sum_{\vec{k}\sigma\vec{k}'\sigma'} \frac{n_{\vec{k}\sigma} - n_{\vec{k}'\sigma'}}{\omega + \varepsilon_{\vec{k}\sigma} - \varepsilon_{\vec{k}'\sigma'} + i\eta} \left(A_{\vec{q}}\right)_{\vec{k}\sigma,\vec{k}'\sigma'} \left(B_{-\vec{q}}\right)_{\vec{k}'\sigma',\vec{k}\sigma} . \tag{2.10}$$

In this thesis, the susceptibilities of interest, denoting specific cases of Eq.(2.10), are mainly the spin-flip susceptibilities χ_{+-}, χ_{-+}. The plus and minus signs denote the corresponding spin-flip operators. The spin density susceptibilities $\chi_{\hat{S}_z\hat{S}_z}, \chi_{\hat{S}_x\hat{S}_x}, \chi_{\hat{S}_y\hat{S}_y}$ will also be considered[9], but not to the same extent. The operators in the subscripts of the aforementioned susceptibilities are defined according to Eq.(2.8), and their corresponding Fourier transforms are given in Eq.(2.9). Using Eq.(2.10) to obtain explicit expression of the aforementioned spin susceptibilities yields

$$\chi^{(0)}_{+-}(\vec{q}, \omega) = \frac{1}{L^d} \sum_{\vec{k}} \frac{n_{\vec{k}\uparrow} - n_{\vec{k}+\vec{q}\downarrow}}{\omega + \varepsilon_{\vec{k}\uparrow} - \varepsilon_{\vec{k}+\vec{q}\downarrow} + i\eta}, \tag{2.11}$$

$$\chi^{(0)}_{-+}(\vec{q}, \omega) = \frac{1}{L^d} \sum_{\vec{k}} \frac{n_{\vec{k}\downarrow} - n_{\vec{k}+\vec{q}\uparrow}}{\omega + \varepsilon_{\vec{k}\downarrow} - \varepsilon_{\vec{k}+\vec{q}\uparrow} + i\eta}, \tag{2.12}$$

$$\chi^{(0)}_{\hat{S}_z\hat{S}_z}(\vec{q}, \omega) = \frac{1}{4L^d} \sum_{\vec{k}\sigma} \frac{n_{\vec{k}\sigma} - n_{\vec{k}+\vec{q}\sigma}}{\omega + \varepsilon_{\vec{k}\sigma} - \varepsilon_{\vec{k}+\vec{q}\sigma} + i\eta}. \tag{2.13}$$

Furthermore, it is easily verified for our model that $\chi^{(0)}_{\hat{S}_x\hat{S}_x}(\vec{q}, \omega) = \chi^{(0)}_{\hat{S}_y\hat{S}_y}$. These susceptibilities can be obtained from the relation[10]

$$\chi^{(0)}_{\hat{S}_x\hat{S}_x}(\vec{q}, \omega) = \frac{1}{4}\left(\chi^{(0)}_{+-}(\vec{q}, \omega) + \chi^{(0)}_{-+}(\vec{q}, \omega)\right).$$

The $\chi_{\hat{S}_x\hat{S}_x}, \chi_{+-}$ and χ_{-+} susceptibilities are called transverse spin-spin response functions. They describe the response of spin density quantities when a magnetic field is applied perpendicularly to the direction of the static spin polarization[11]. Similarly, $\chi_{\hat{S}_z\hat{S}_z}$ is referred to as a longitudinal spin susceptibility, as it describes the response of the z-component of the spin density subject to the application of a magnetic field in parallel with the static spin polarization. A noteworthy property of the spin-flip susceptibilities is

$$\chi^{(0)}_{+-}(\vec{q}, \omega) = \left(\chi^{(0)}_{-+}(\vec{q}, -\omega)\right)^*, \tag{2.14}$$

To analytically evaluate the expressions in Eqs.(2.11)-(2.13), we cast the sum over $\vec{k}$ into an integral according to $\sum_k \to \frac{L^d}{(2\pi)^d} \int d\vec{k}$. Followed by algebraic manipulations[11], we obtain

[9] Here, the dependence on momentum and frequency, in addition to the superscripts were dropped for brevity.

[10] See Sec.6.6 in the appendix for the full details on deriving the susceptibilities and relevant relations.

[11] See Sec. 6.7 in the appendix for the full details.

that the imaginary parts of the considered spin susceptibilities are given by

$$\mathrm{Im}\chi^{(0)}_{+-}(\vec{q},\omega) = C\left[\int_{n_{\vec{k}\uparrow}=1} d\vec{k}\delta(\omega+\varepsilon_{\vec{k}\uparrow}-\varepsilon_{\vec{k}+\vec{q}\downarrow}) - \int_{n_{\vec{k}\downarrow}=1} d\vec{k}\delta(\omega+\varepsilon_{\vec{k}-\vec{q}\uparrow}-\varepsilon_{\vec{k}\downarrow})\right], \quad (2.15)$$

$$\mathrm{Im}\chi^{(0)}_{-+}(\vec{q},\omega) = C\left[\int_{n_{\vec{k}\downarrow}=1} d\vec{k}\delta(\omega+\varepsilon_{\vec{k}\downarrow}-\varepsilon_{\vec{k}+\vec{q}\uparrow}) - \int_{n_{\vec{k}\uparrow}=1} d\vec{k}\delta(\omega+\varepsilon_{\vec{k}-\vec{q}\downarrow}-\varepsilon_{\vec{k}\uparrow})\right], \quad (2.16)$$

$$\mathrm{Im}\chi^{(0)}_{\hat{S}_z\hat{S}_z}(\vec{q},\omega) = \frac{C}{4}\sum_{\sigma}\int_{n_{\vec{k}\sigma}=1}\left[\delta(\omega+\varepsilon_{\vec{k}\sigma}-\varepsilon_{\vec{k}+\vec{q}\sigma}) - \delta(\omega+\varepsilon_{\vec{k}-\vec{q}\sigma}-\varepsilon_{\vec{k}\sigma})\right] d\vec{k}. \quad (2.17)$$

where $C = -\frac{\pi}{(2\pi)^d}$, and d is the dimensionality, which we take to be $d = 2$.

3 Method

3.1 Spin-flip susceptibilities for the non-altermagnets

Before computing spin-flip susceptibilities for the altermagnetic phase, we consider the simpler task of evaluating spin-flip susceptibilities for a dispersion relation modelling a two dimensional non-altermagnetic phase.

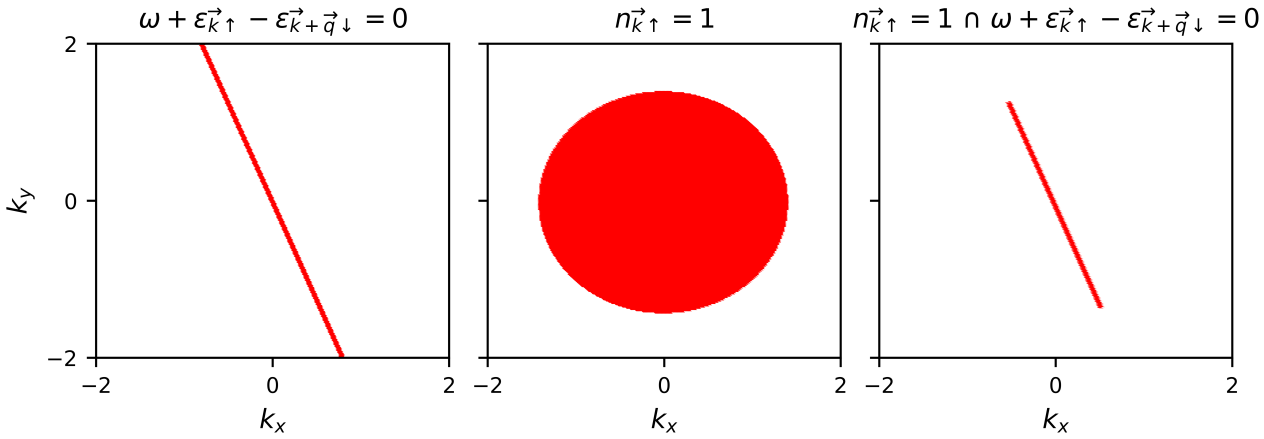

Figure 4: The leftmost panel depicts the curve $\delta(\omega+\varepsilon_{\vec{k}\uparrow}-\varepsilon_{\vec{k}+\vec{q}\downarrow})$ for the non-altermagnetic dispersion. The middle panel displays the Fermi volume, and the rightmost panel displays the intersection of the two aforementioned regions. The rightmost panel determines the integration region
. The parameters used in producing the plots were $m = 1, \mu = 1, \omega = 0.15, q_x = 0.5$ and $q_y = 0.2$.

By a non-altermagnetic phase, we mean a magnetic phase with a spin degenerate dispersion relation. As such, we consider the dispersion relation

$$\varepsilon(\vec{k}) = \frac{k_x^2 + k_y^2}{2m}.$$

This calculation has been considered in literature [11], but it usually relies on exploiting rotational symmetry. Since rotational symmetry cannot be assumed when performing similar calculations for altermagnets, we wish to avoid it. Consider the integral

$$\int_{n_{\vec{k}\uparrow}=1} d\vec{k}\delta(\omega + \varepsilon_{\vec{k}\uparrow} - \varepsilon_{\vec{k}+\vec{q}\downarrow}). \tag{3.1}$$

The presence of the Dirac delta restricts the integration region to the curve $\omega+\varepsilon_{\vec{k}\uparrow}-\varepsilon_{\vec{k}+\vec{q}\downarrow} = 0$ inside of the Fermi volume, $n_{\vec{k}\uparrow} = 1$. Computing the integral in Eq. (3.1) is geometrically equivalent to determining the arc-length of the curve $\omega + \varepsilon_{\vec{k}\uparrow} - \varepsilon_{\vec{k}+\vec{q}\downarrow} = 0$ inside of the Fermi surface. These curves are depicted in Fig. 4. The Fermi surface is determined by $\mu = \frac{k_x^2+k_y^2}{2m}$, where μ is the chemical potential of the metal. For brevity, $\sqrt{2m\mu} = k_F$. Letting $f(k_x, k_y) = \omega + \varepsilon_{\vec{k}\uparrow} - \varepsilon_{\vec{k}+\vec{q}\downarrow}$,

$$\begin{aligned} f(k_x, k_y) &= \omega - \frac{k_x q_x}{m} - \frac{k_y q_y}{m} - \frac{q_x^2 + q_y^2}{2m}, \\ f(k_x, k_y) = 0 \Rightarrow k_y(k_x) &= \frac{m}{q_y}\left(\omega - \frac{k_x q_x}{m} - \frac{q_x^2 + q_y^2}{2m}\right). \end{aligned}$$

Note how $k_y(k_x)$ is linear in k_x, which is seen in the leftmost and rightmost panels in Fig. 4. For fixed k_x, we may use the Dirac delta decomposition[14]

$$\delta[f(k_x, k_y)] = \sum_i \frac{\delta(k_y - k_{y,i}(k_x))}{\left|\frac{\partial}{\partial k_y} f(k_x, k_y)|_{k_y = k_{y,i}(k_x)}\right|}, \quad f(k_x, k_{y,i}(k_x)) = 0. \tag{3.2}$$

In Eq. (3.2), the sum is taken over all possible solutions i of k_y in terms of k_x. Carrying out the integral,

$$\begin{aligned} \int_{n_{\vec{k}\uparrow}=1} d\vec{k}\delta(\omega + \varepsilon_{\vec{k}\uparrow} - \varepsilon_{\vec{k}+\vec{q}\downarrow}) &= \frac{m}{|q_y|}\int_{-k_F}^{k_F}\int_{-\sqrt{k_F^2-k_x^2}}^{\sqrt{k_F^2-k_x^2}} \delta(k_y - k_y(k_x)) dk_y dk_x, \\ &= \frac{m}{|q_y|}\int_{-k_F}^{k_F} \Theta\left(k_y(k_x) + \sqrt{k_F^2 - k_x^2}\right)\Theta\left(\sqrt{k_F^2 - k_x^2} - k_y(k_x)\right) dk_x. \end{aligned}$$

The product of the theta functions can be simplified as

$$\Theta\left(k_y(k_x) + \sqrt{k_F^2 - k_x^2}\right)\Theta\left(\sqrt{k_F^2 - k_x^2} - k_y(k_x)\right) = \Theta\left(k_F^2 - k_x^2 - [k_y(k_x)]^2\right),$$

which will determine the integration boundaries. Solving $k_F^2 - k_x^2 - [k_y(k_x)]^2 = 0$ for k_x gives

$$k_{x,\pm} = \frac{-q_x\left(q^2 - 2m\omega\right) \pm q_y\sqrt{4k_F^2 q^2 - \left(q^2 - 2m\omega\right)^2}}{2q^2}.$$

Real solutions only exist provided $4k_F^2q^2-(q^2-2m\omega)^2>0$, which geometrically corresponds to the curve $f(k_x,k_y)=0$ having two intersection points with the Fermi surface. If $4k_F^2q^2-(q^2-2m\omega)^2\leq 0$, there is one, or no intersection points of $f(k_x,k_y)=0$ with the Fermi surface, so the integral is zero. Assuming $4k_F^2q^2-(q^2-2m\omega)^2>0$ and $q_y>0$,

$$\int_{n_{\vec{k}\uparrow}=1} d\vec{k}\delta(\omega+\varepsilon_{\vec{k}\uparrow}-\varepsilon_{\vec{k}+\vec{q}\downarrow})=\frac{2mk_F}{q}\sqrt{1-\left(\frac{\omega}{qv_F}-\frac{q}{2k_F}\right)^2},$$

where $v_F=\frac{k_F}{m}$. Performing the other integral in a similar fashion results in

$$\mathrm{Im}\chi^{(0)}_{+-}(\vec{q},\omega)=-\frac{mk_F}{2\pi q}\left(\sqrt{1-\nu_-^2}\Theta(1-\nu_-^2)-\sqrt{1-\nu_+^2}\Theta(1-\nu_+^2)\right), \tag{3.3}$$

where $\nu_\pm=\frac{\omega}{qv_F}\pm\frac{q}{2k_F}$. Eq. (3.3) is a known literature result [11]. In general, dispersion relations with spin degeneracy will show no splitting between the imaginary parts of the spin-flip susceptibilities, as Eqs. (2.15) and (2.16) are equivalent in this case. The theta functions in Eq. (3.3) ensure that the susceptibility is zero outside of its range of allowed values.

3.2 Spin-flip susceptibilities for altermagnets along cardinal directions

The main novel part of this thesis is dedicated towards computing the imaginary part of the spin-flip susceptibilities using the simple minimal model of the dispersion relation of a non-interacting altermagnetic electron gas, modelled as

$$\varepsilon(\sigma,\vec{k})=\delta_{\sigma\uparrow}\left(\frac{k_x^2}{2m_1}+\frac{k_y^2}{2m_2}\right)+\delta_{\sigma\downarrow}\left(\frac{k_y^2}{2m_1}+\frac{k_x^2}{2m_2}\right). \tag{3.4}$$

The four integrals involved in computing the spin susceptibilities , given in Eqs. (2.15) and (2.16), can be obtained in almost identical ways. As such, detailed calculations of only one of the integrals will be given. We will assume $m_1>m_2, T=0$ and consider $\vec{q}$ to be along cardinal directions to avoid computational complexity, meaning $\vec{q}=(q_x,0)$ or $\vec{q}=(0,q_y)$. We will specifically consider $\vec{q}=(0,q_y)$.

The dispersion relation modelling the altermagnetic phase in Eq. (3.4) is associated with two spin-dependent Fermi volumes. These regions are determined by the spin-dependent particle density at $T=0$ which is denoted by $n_{\vec{k}\sigma}$. Spin up electrons are confined to states within the Fermi volume $n_{\vec{k}\uparrow}=1$, which has Fermi surface $\mu=\frac{k_x^2}{2m_1}+\frac{k_y^2}{2m_2}$. Here, μ is the chemical potential of the metal. Analogously, the Fermi volume for spin down electrons is given by $n_{\vec{k}\downarrow}=1$, which has Fermi surface $\mu=\frac{k_x^2}{2m_2}+\frac{k_y^2}{2m_1}$. The Fermi surfaces for the different spin branches are ellipses in momentum space, connected by a 90° degree rotation.

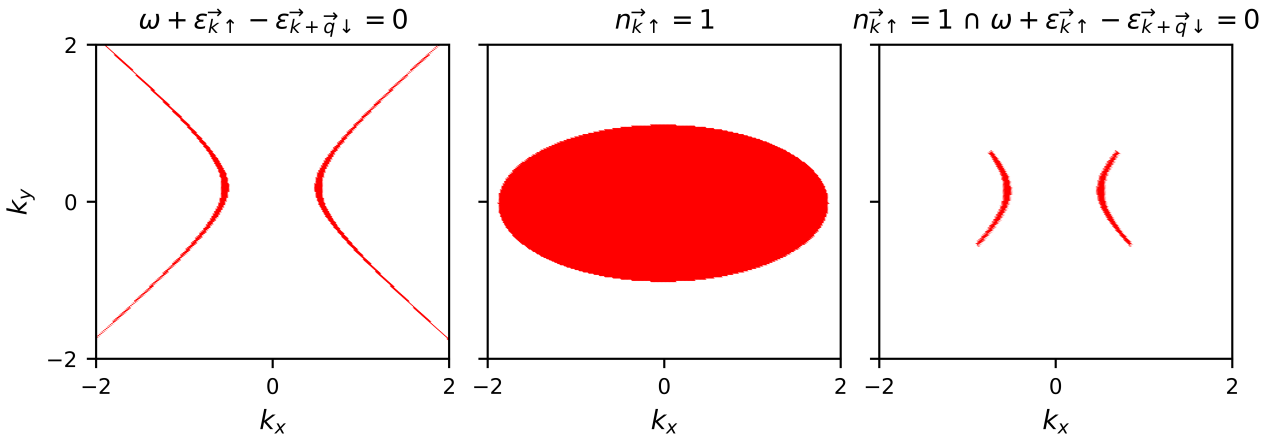

Figure 5: The leftmost panel depicts the curve $\delta(\omega + \varepsilon_{\vec{k}\uparrow} - \varepsilon_{\vec{k}+\vec{q}\downarrow})$ for the altermagnetic dispersion. The middle panel displays the Fermi volume, and the rightmost panel displays the intersection of the two aforementioned regions
. The parameters used in producing the plots were
$\omega = 0.15, q_x = 0, q_y = 0.5, \mu = 0.5, m_1 = 3.5$ and $m_2 = 1$. For these values, $K_- > 0$, or $\omega > \frac{q_y^2}{2(m_1 - m_2)}$.

3.2.1 Computing $\int_{n_{\vec{k}\uparrow}=1} d\vec{k}\delta(\omega + \varepsilon_{\vec{k}\uparrow} - \varepsilon_{\vec{k}+\vec{q}\downarrow})$

Consider the $\mathrm{Im}\chi^{(0)}_{+-}(\vec{q}, \omega)$ susceptibility, and the first integral in Eq. (2.15), specifically

$$\int_{n_{\vec{k}\uparrow}=1} d\vec{k}\delta(\omega + \varepsilon_{\vec{k}\uparrow} - \varepsilon_{\vec{k}+\vec{q}\downarrow}), \tag{3.5}$$

where $\varepsilon(\vec{k}, \sigma)$ is the altermagnetic dispersion relation from Eq. (3.4). Letting $f(k_x, k_y) = \varepsilon_{\vec{k}\uparrow} - \varepsilon_{\vec{k}+\vec{q}\downarrow} + \omega$, Fig. 5 displays that $f(k_x, k_y) = 0$ forms a hyperbola in momentum space. Computing the integral in Eq. (3.5) is geometrically equivalent to calculating the arc-length of the hyperbola $f(k_x, k_y) = 0$ inside of the Fermi volume. These curves are depicted in Fig. 5.

In order to avoid broken integration domains, the first integral of the double integral in Eq. (3.5) involves the decomposed Dirac delta. This first integral ought to be taken along the coordinate axis which is parallel to the major axis of the hyperbola $f(k_x, k_y) = 0$. The region where the hyperbola does not exist will then effectively be "integrated out" by the Dirac delta, ensuring no broken integration domains have to be considered in the second integral of the double integral. Hence, we begin by factoring $f(k_x, k_y)$ into hyperbolic form to obtain a condition determining the direction of its major axis. We introduce the following change of variables to reflect the geometric shape of the hyperbola,

$$M = \frac{m_1 m_2}{m_1 - m_2}, Y_i = \frac{m_i q_y}{m_1 - m_2}, K_\pm = \omega \pm \frac{q_y^2}{2(m_1 - m_2)}, R = \frac{m_1 m_2}{m_1 + m_2},$$

where $i = 1, 2$. Note that the introduction of the reduced mass R, allows us to express m_1 and m_2 as

$$m_1 = \frac{2MR}{M-R}\ ,\ m_2 = \frac{2MR}{M+R}. \tag{3.6}$$

Then,

$$f(k_x, k_y) = -\frac{k_x^2}{2M} + \frac{(k_y - Y_2)^2}{2M} + K_-.$$

The curve $\delta(\omega + \varepsilon_{\vec{k}\uparrow} - \varepsilon_{\vec{k}+\vec{q}\downarrow})$ corresponds to $f(k_x, k_y) = 0$, given by the hyperbola

$$\frac{k_x^2}{2M} - \frac{(k_y - Y_2)^2}{2M} = K_-. \tag{3.7}$$

Geometrically, Y_i determines the position of the center of the hyperbola, given by $(0, Y_i)$. By setting $q_x = 0$, no horizontal translation of the hyperbola is allowed.

The sign of K_- determines the orientation of the major axis. For $K_- = 0$, $f(k_x, k_y) = 0$ consists of four connected line segments. No case distinction is needed for $K_- = 0$. The integration order does not matter since there is no undefined region. Then,

$$K_- \geq 0 \Rightarrow \text{ Major axis is along } k_y = Y_2 \Rightarrow \text{ Integrate over } k_x \text{ first.} \tag{3.8}$$
$$K_- \leq 0 \Rightarrow \text{ Major axis is along } k_x = 0 \Rightarrow \text{ Integrate over } k_y \text{ first.} \tag{3.9}$$

Case I: Suppose $K_- \geq 0$, meaning we ought to integrate over k_x according to Eq. (3.8). The integrand $\delta(\omega + \varepsilon_{\vec{k}\uparrow} - \varepsilon_{\vec{k}+\vec{q}\downarrow})$ is simplified using the decomposition

$$\delta[f(k_x, k_y)] = \sum_i \frac{\delta(k_x - k_{x,i}(k_y))}{\left|\frac{\partial}{\partial k_x} f(k_x, k_y)|_{k_x = k_{x,i}(k_y)}\right|}, \quad f(k_{x,i}(k_y), k_y) = 0,$$

for fixed k_y. From Eq. (3.7),

$$k_{x,\pm}(k_y) = \pm\sqrt{(k_y - Y_2)^2 + 2K_-M}.$$

Note, $k_{x,\pm}(k_y)$ only exists provided $(k_y - Y_2)^2 \geq -2K_-M$. This is trivially satisfied as $K_- \geq 0$ is assumed, and $M > 0$ always holds true provided $m_1 > m_2$. Letting $k_x(k_y) = k_{x,+}(k_y)$, then $k_{x,-}(k_y) = -k_x(k_y)$, and the Dirac delta decomposition is given by

$$\delta(\omega + \varepsilon_{\vec{k}\uparrow} - \varepsilon_{\vec{k}+\vec{q}\downarrow}) = M\frac{\delta(k_x - k_x(k_y)) + \delta(k_x + k_x(k_y))}{\sqrt{(k_y - Y_2)^2 + 2K_-M}}.$$

This allows us to express the integral as

$$\int_{n_{\vec{k}\uparrow}=1, K_- \geq 0} d\vec{k}\,\delta(\omega + \varepsilon_{\vec{k}\uparrow} - \varepsilon_{\vec{k}+\vec{q}\downarrow})$$
$$= M\int_{-\sqrt{2m_2\mu}}^{\sqrt{2m_2\mu}} \int_{-\sqrt{2m_1\mu - \frac{m_1}{m_2}k_y^2}}^{\sqrt{2m_1\mu - \frac{m_1}{m_2}k_y^2}} \frac{\delta(k_x - k_x(k_y)) + \delta(k_x + k_x(k_y))}{\sqrt{(k_y - Y_2)^2 + 2K_-M}} dk_x dk_y.$$

As the integration region is symmetric over k_x, and the delta peaks are positioned at $k_x = -k_x(k_y)$ and $k_x = k_x(k_y)$, the conditions for the delta peaks to be inside of the integration region are the same for both peaks. Then, we can use the property $\Theta(a+c)\Theta(a-c) = \Theta(a^2-c^2)$ to obtain

$$\int_{n_{\vec{k}\uparrow}=1, K_- \geq 0} d\vec{k}\delta(\omega + \varepsilon_{\vec{k}\uparrow} - \varepsilon_{\vec{k}+\vec{q}\downarrow}) = 2M \int_{-\sqrt{2m_2\mu}}^{\sqrt{2m_2\mu}} \frac{\Theta\left(2m_1\mu - \frac{m_1}{m_2}k_y^2 - k_x(k_y)^2\right)}{\sqrt{(k_y - Y_2)^2 + 2K_-M}} dk_y. \quad (3.10)$$

The theta function in Eq. (3.10) determines the values of k_y where the integral is non-zero, and by extension the integration boundaries. To find the integration boundaries, we solve for the values of k_y for which

$$2m_1\mu - \frac{m_1}{m_2}k_y^2 - k_x(k_y)^2 \geq 0 \iff \mu \geq \frac{k_x(k_y)^2}{2m_1} + \frac{k_y^2}{2m_2}.$$

This is geometrically equivalent to determining the values of k_y where $\delta(\omega + \varepsilon_{\vec{k}\uparrow} - \varepsilon_{\vec{k}+\vec{q}\downarrow})$ is inside of the Fermi volume $n_{\vec{k}\uparrow} = 1$. Instead of explicitly introducing m_1 and m_2 into the equations, we use their expressions in terms of M, R, given in Eq. (3.6). Then, we only have to introduce two variables (R and μ) as opposed to three (m_1, m_2 and μ) into the equations. The inequality determining the integration boundaries is then given by

$$\mu \geq \frac{k_x^2(k_y)(M-R)}{4MR} + \frac{k_y^2(M+R)}{4MR}. \quad (3.11)$$

Solving the inequality in Eq. (3.11) yields $k_{1,-} \leq k_y \leq k_{1,+}$ where

$$k_{1,\pm} = \frac{Y_2(M-R) \pm \sqrt{-4K_-M^2(M-R) + 8\mu M^2 R - Y_2^2(M^2-R^2)}}{2M}. \quad (3.12)$$

Here, $k_{1,\pm}$ represents the k_y-coordinates of the intersection points between the curve $\delta(\omega + \varepsilon_{\vec{k}\uparrow} - \varepsilon_{\vec{k}+\vec{q}\downarrow})$ and the Fermi surface. In general, the number of intersection points depends on the relative geometry between the Fermi surface and the hyperbola. The allowed degrees of freedom of the hyperbola, meaning k_x and k_y translation, also affects the number of intersection points. For the considered case, corresponding to Eq. (3.12), two intersection points were obtained. Geometrically, this means that no matter the horizontal translation of the hyperbola (determined by Y_2), its two branches will intersect the Fermi surface at the same k_y coordinates. This can be observed in Fig. 5.

Provided $k_{1,\pm}$ is real and $k_{1,+} \neq k_{1,-}$, the integral is non-zero with integration bounds $k_y \in [k_{1,-}, k_{1,+}]$. Otherwise the integral is zero or does not exist in the sense of being complex. Then[12],

$$\begin{aligned}\int_{n_{\vec{k}\uparrow}=1, K_- \geq 0} d\vec{k}\ \delta(\omega + \varepsilon_{\vec{k}\uparrow} - \varepsilon_{\vec{k}+\vec{q}\downarrow}) &= 2M \int_{k_{1,-}}^{k_{1,+}} \frac{1}{\sqrt{(k_y - Y_2)^2 + 2K_-M}}\, dk_y, \\ &= 2M \left[\log\left(\sqrt{2K_-M + (k_y - Y_2)^2} + (k_y - Y_2)\right)\right]_{k_{1,-}}^{k_{1,+}}.\end{aligned}$$

[12]This is a reoccurring integral. The details of obtaining the indefinite integral can be found in Sec. 6.8 in the appendix.

For brevity, we introduce the variable $P_{\pm}^2 = 2MK_{\pm}$. When it is real, $2\sqrt{\pm 2MK_+}$ corresponds to the distance between the vertices of the hyperbola $f(k_x, k_y) = 0$. Provided $k_{1,\pm}$ is real[13], the definite integral is given by

$$\int_{n_{\vec{k}\uparrow}=1, K_- \geq 0} d\vec{k}\ \delta(\omega + \varepsilon_{\vec{k}\uparrow} - \varepsilon_{\vec{k}+\vec{q}\downarrow}) = 2M \log\left(\frac{\sqrt{P_-^2 + (k_{1,+} - Y_2)^2} + (k_{1,+} - Y_2)}{\sqrt{P_-^2 + (k_{1,-} - Y_2)^2} + (k_{1,-} - Y_2)}\right).$$

Case II: Suppose $K_- \leq 0$. As prescribed by Eq. (3.9), we ought to integrate over k_y first to avoid broken integration domains in the second integral.

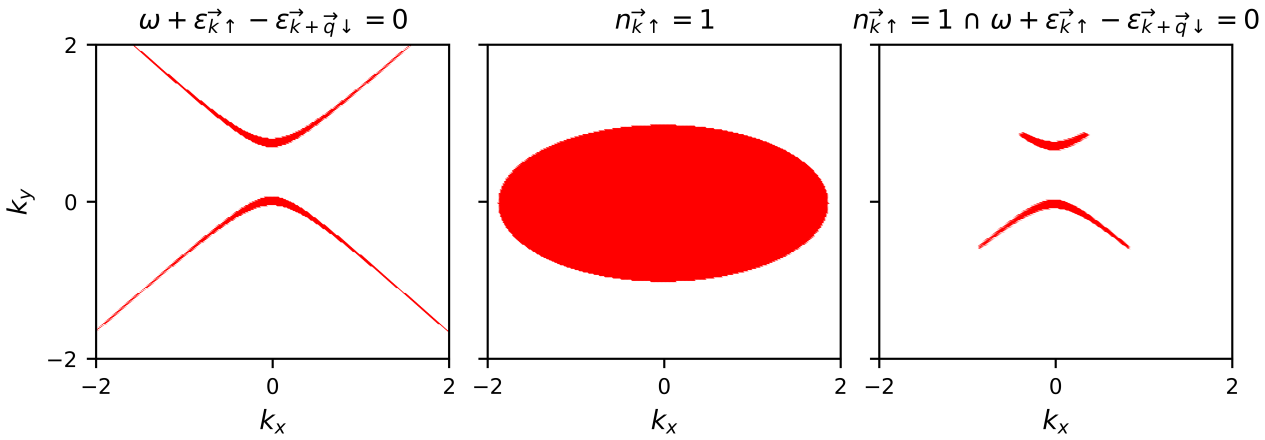

Figure 6: The leftmost panel depicts the curve $\delta(\omega + \varepsilon_{\vec{k}\uparrow} - \varepsilon_{\vec{k}+\vec{q}\downarrow})$, for the altermagnetic dispersion. The middle panel displays the Fermi volume, and the rightmost panel displays the intersection of the two aforementioned regions. The parameters used in producing the plots were $\omega = 0.15, q_x = 0, q_y = 1, \mu = 0.5, m_1 = 3.5$ and $m_2 = 1$. For these values, $K_- < 0$, or $\omega < \frac{q_y^2}{2(m_1 - m_2)}$.

The integrand $\delta(\omega + \varepsilon_{\vec{k}\uparrow} - \varepsilon_{\vec{k}+\vec{q}\downarrow})$ is simplified using the Dirac delta decomposition given by Eq. (3.2), where

$$k_{y,\pm}(k_x) = Y_2 \pm \sqrt{k_x^2 - 2MK_-}.$$

Note that $k_{y,\pm}(k_x)$ is real, since $K_- \leq 0$ is assumed, and $M > 0$ holds provided $m_1 > m_2$. Then,

$$\delta(\omega + \varepsilon_{\vec{k}\uparrow} - \varepsilon_{\vec{k}+\vec{q}\downarrow}) = M\frac{\delta(k_y - k_{y,-}(k_x)) + \delta(k_y - k_{y,+}(k_x))}{\sqrt{k_x^2 - 2MK_-}}.$$

[13]The statement "provided $k_{1,\pm}$ is real" can be mathematically stated in terms of a theta function, which is done in Eq. (3.3). We do not write the theta function here for brevity.

Hence, we are integrating

$$\int_{n_{\vec{k}\uparrow}=1,K_-\leq 0} d\vec{k}\ \delta(\omega+\varepsilon_{\vec{k}\uparrow}-\varepsilon_{\vec{k}+\vec{q}\downarrow}) = M\int_{-\sqrt{2m_1\mu}}^{\sqrt{2m_1\mu}} \frac{\Theta\left(\mu-\frac{k_x^2}{2m_1}-\frac{k_{y,-}(k_x)^2}{2m_2}\right)}{\sqrt{k_x^2-2MK_-}}+\frac{\Theta\left(\mu-\frac{k_x^2}{2m_1}-\frac{k_{y,+}(k_x)^2}{2m_2}\right)}{\sqrt{k_x^2-2MK_-}}\ dk_x.$$

Using the expression for the effective masses m_1 and m_2 in terms of M and R , as given in Eq. (3.6), and subsequently solving for k_x in inequalities

$$\mu \geq \frac{k_x^2(M-R)}{4MR}+\frac{k_{y,+}(k_x)^2(M+R)}{4MR} \text{ and } \mu \geq \frac{k_x^2(M-R)}{4MR}+\frac{k_{y,-}(k_x)^2(M+R)}{4MR},$$

yields the two inequalities $k_{1,-,-}\leq k_x\leq k_{1,+,-}$ and $k_{1,-,+}\leq k_x\leq k_{1,+,+}$. Here,

$$k_{1,\pm,\pm}=\pm\sqrt{\frac{(M+R)[|Y_2|\,(2Mk_{1,\pm}-Y_2(M-R))+2K_-M^2+Y_2^2R]+4\mu M^2R}{2M^2}},$$

and the expression for $k_{1,\pm}$ is given in Eq. (3.12). The first $\pm$-sign in $k_{1,\pm,\pm}$ determines the sign of the square root, and the second $\pm$-sign determines the sign of $k_{1,\pm}$.

It is assumed that $K_-\leq 0$, meaning the major axis of $f(k_x,k_y)=0$ is along $k_x=0$. Since $q_x=0$, the hyperbola $f(k_x,k_y)=0$ cannot be horizontally translated in momentum space. Therefore, the k_x-coordinates of the intersection points between one branch of the hyperbola and the Fermi surface will differ in sign only. This observation can be seen in Fig. 6. Provided $k_{1,\pm,+}$ and $k_{1,\pm,-}$ are real[14], the definite integral is given by

$$\int_{n_{\vec{k}\uparrow}=1,K_-\leq 0} d\vec{k}\delta(\omega+\varepsilon_{\vec{k}\uparrow}-\varepsilon_{\vec{k}+\vec{q}\downarrow}) = M\int_{k_{1,-,-}}^{k_{1,+,-}}\frac{1}{\sqrt{k_x^2-2MK_-}}\ dk + M\int_{k_{1,-,+}}^{k_{1,+,+}}\frac{1}{\sqrt{k_x^2-2MK_-}}\ dk_x,$$

$$= M\log\left(\frac{\sqrt{k_{1,+,-}^2-P_-^2}+k_{1,+,-}}{\sqrt{k_{1,-,-}^2-P_-^2}+k_{1,-,-}}\right)+M\log\left(\frac{\sqrt{k_{1,+,+}^2-P_-^2}+k_{1,+,+}}{\sqrt{k_{1,-,+}^2-P_-^2}+k_{1,-,+}}\right).$$

Then, the complete integral is

$$\int_{n_{\vec{k}\uparrow}=1} d\vec{k}\delta(\omega+\varepsilon_{\vec{k}\uparrow}-\varepsilon_{\vec{k}+\vec{q}\downarrow}) = \int_{n_{\vec{k}\uparrow}=1,K_-\leq 0} d\vec{k}\delta(\omega+\varepsilon_{\vec{k}\uparrow}-\varepsilon_{\vec{k}+\vec{q}\downarrow}) + \int_{n_{\vec{k}\uparrow}=1,K_-\geq 0} d\vec{k}\delta(\omega+\varepsilon_{\vec{k}\uparrow}-\varepsilon_{\vec{k}+\vec{q}\downarrow}).$$

[14]These conditions may also be written in terms of theta functions.

Of particular interest are the curves determining where the integration boundaries become complex. These are readily solved for as

$$\omega_{1,0} = \frac{k_{F,1}^2}{2m_2} + \frac{q_y^2}{2m_2}\left(\frac{m_1 m_2}{m_1^2 - m_2^2}\right) - \frac{k_{F,1}^2}{2m_1}, \tag{3.13}$$

$$\omega_{1,\pm} = \frac{\left(k_{F,2} \pm |q_y|\right)^2}{2m_1} - \frac{k_{F,2}^2}{2m_2}. \tag{3.14}$$

Here, we introduced the variables $k_{F,1} = \sqrt{2m_1\mu}$ and $k_{F,1} = \sqrt{2m_2\mu}$, corresponding to the lengths of the axes of the ellipsoidal Fermi surface. Physically, the lines in Eqs. (3.13) and (3.14) determine limiting, or special excitation processes. These lines, and their physical implications are discussed in Sec. 4.2.

As previously noted, the remaining three double integrals involved in the determining the spin-flip susceptibilities may be evaluated in an identical way to that presented in this section. In Sec. 6.9 in the appendix, we state the results for the remaining integrals. It should be noted that the integrals in Eq. (2.16) can be obtained by simple changes of variables from the integrals calculated in Eq. (2.15).

3.3 Longitudinal spin susceptibility for altermagnets

The imaginary part of the longitudinal spin susceptibility for the altermagnetic dispersion relation was also calculated. That is, the integrals in Eq. (2.17) using the dispersion relation in Eq. (6.1) were evaluated. As the terms in the integrals involved in Eq. (2.17) are confined to the same spin branch of the dispersion relation, the calculations are essentially identical to those performed in Sec. 3.1. Specifically, the curves $\delta(\omega + \varepsilon_{\vec{k}\sigma} - \varepsilon_{\vec{k}+\vec{q}\sigma})$ and $\delta(\omega + \varepsilon_{\vec{k}-\vec{q}\sigma} - \varepsilon_{\vec{k}\sigma})$ form lines in momentum space, as opposed to hyperbolas. The full algebraic details are provided in Sec. 6.10 in the appendix, where the susceptibility is obtained as

$$\begin{aligned}\mathrm{Im}\chi^{(0)}_{\hat{S}_z\hat{S}_z}(\vec{q},\omega) = -\frac{\pi}{4(2\pi)^2}\sum_{\sigma}\Bigg[&\sqrt{\frac{4m_i^2 m_{\bar{i}}^2(2\mu+\omega)}{m_i q_y^2 + m_{\bar{i}} q_x^2} - \frac{4m_i^3 m_{\bar{i}}^3\omega^2}{\left(m_i q_y^2 + m_{\bar{i}} q_x^2\right)^2} - m_i m_{\bar{i}}} \\ &- \sqrt{\frac{4m_i^2 m_{\bar{i}}^2(2\mu-\omega)}{m_i q_y^2 + m_{\bar{i}} q_x^2} - \frac{4m_i^3 m_{\bar{i}}^3\omega^2}{\left(m_i q_y^2 + m_{\bar{i}} q_x^2\right)^2} - m_i m_{\bar{i}}}\Bigg].\end{aligned} \tag{3.15}$$

We may then easily take the limit $m_i \to m_{\bar{i}} \to m$ to recover a similar result to that obtained in Sec. 3.1. In this case, Eqs. (3.15) and (3.3) are identical up to a factor of 2. We obtain this result as the dispersion relation is spin degenerate in the limit $\lim_{m_i \to m_{\bar{i}}}$, which means that Eqs. (2.16) and (2.17) only differ by a factor of 2, as obtained. The origin of the factor of 2 stems from the absence of correlations between spin up and spin down electrons. In this case, $\chi^{(0)}_{\hat{S}_z\hat{S}_z}(\vec{q},\omega) = \chi^{(0)}_{\uparrow\uparrow}(\vec{q},\omega) + \chi^{(0)}_{\downarrow\downarrow}(\vec{q},\omega)$, where $\chi^{(0)}_{\sigma_1\sigma_2}(\vec{q},\omega)$ is the spin-resolved density-density susceptibility[15][11]. Apart from two spin-dependent branches appearing in the excitation spectrum, the results closely resemble those for the non-altermagnetic case. As such, the results for the longitudinal spin susceptibility will not be further considered as part of the

[15]For the definition of the spin-resolved density-density susceptibility, see chapter 3.5 in [11].

main thesis. However, detailed considerations are given in Sec. 6.12 in the appendix for the interested reader.

3.4 Numerical comparisons with analytical results

To confirm the validity of the analytical results, a numerical approach was also considered. Specifically discretized Riemann sums of the considered integrals were carried out. The results are displayed in Fig. 7.

The delta function was discretized using $|\omega + \varepsilon_{\vec{k}\uparrow} - \varepsilon_{\vec{k}+\vec{q}\downarrow}| \leq \eta$ for an appropriately small linewidth $\eta \geq 0$. If the linewidth is chosen too large, features of the curves displayed in the upper panels of Fig. 7 become lost, and if the linewidth is chosen too small, the curves become distorted. The resulting curves from the discretized integration were divided by 2η (total linewidth) to obtain the appropriate scaling.

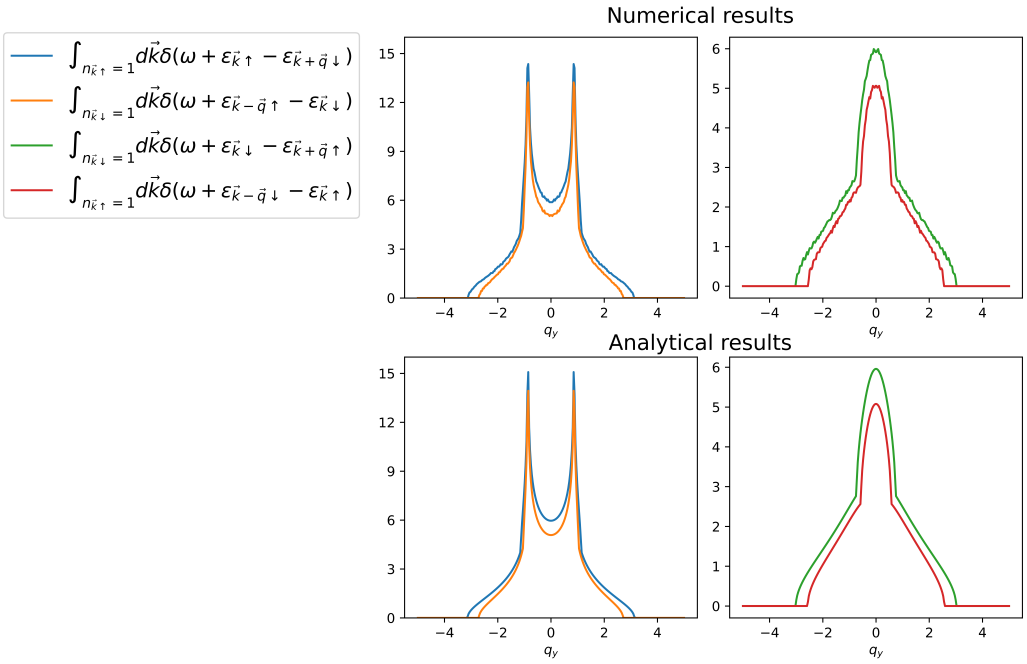

Figure 7: Comparison between analytical and numerical results. The parameters used were $m_1 = 3.5, m_2 = 1, \mu = 0.5$ and $\omega = 0.15$. For the numerical approach, each grid point occupied an area of $1.3 \cdot 10^{-4}$ units^2, and the line-width was set to be 0.030 units. The vertical axis determines the magnitude of the integrals.

The numerical and analytical results align well, and the comparison strengthens the validity of the analytical results. In the left panels of Fig. 7, the peaks of the curves for the analytical and numerical results differ slightly. This is a consequence of sharp features being lost during discretization.

4 Numerical results and discussion

Having obtained explicit expressions for the imaginary part of the spin-flip susceptibilities, we examine them further by studying their dependence on momentum and energy transfers (q_y, ω) from heat maps. The lines plotted in the heat maps, and subsequently the marked points of the cross sections, mark regions where non-analytic features are expected. That is, lines correspond to those given in Eqs. (3.13) and (3.14) for all of the involved integrals. All displayed results were obtained using $\mu = 0.5$.

The heat maps depict the magnetic excitation spectra of electrons[16]. Elementary excitations are obtained by magnetic interactions transferring energy ω and momentum $\vec{q}$ to an electron at a state $\vec{k}\sigma_1$ inside of the Fermi surface, causing the electron to be displaced to a state $\vec{k}+\vec{q}\sigma_2$ outside of the Fermi surface. This process creates a hole at the previously occupied state. As will be discussed, features of the excitation spectrum depend on the geometry of the Fermi surface.

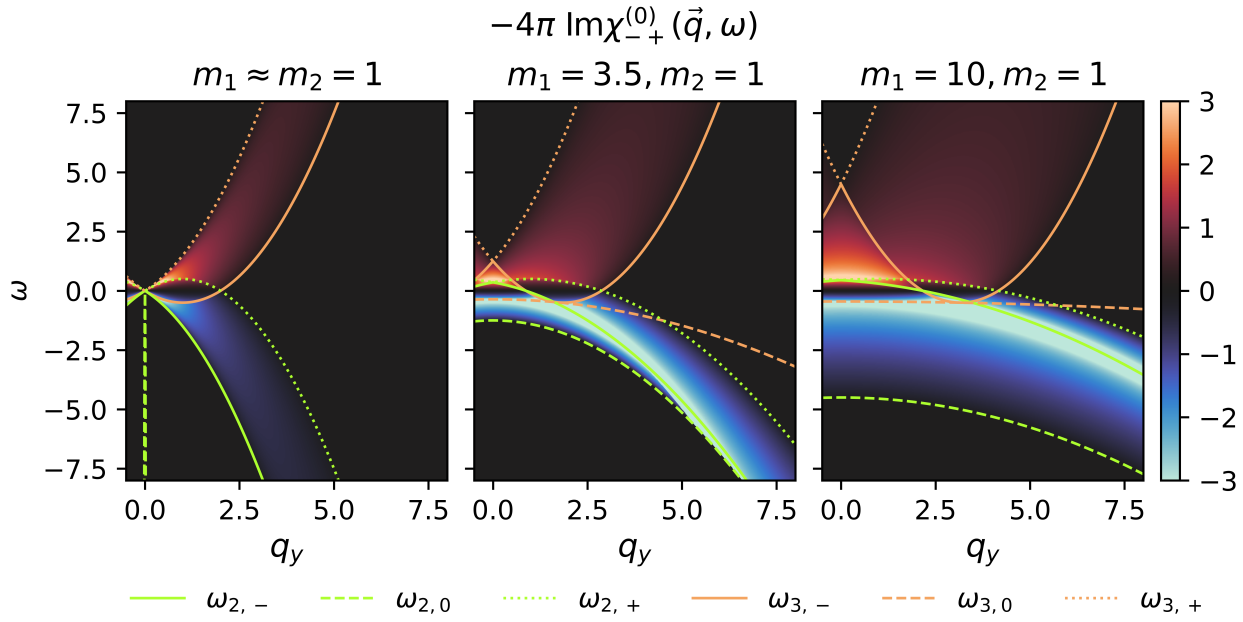

Figure 8: Imaginary part of $\chi^{(0)}_{-+}(\vec{q},\omega)$, displayed for different pairs of effective electron masses. As $\mathrm{Im}\chi^{(0)}_{-+}(\vec{q},\omega)$ is symmetric with respect to q_y, it is plotted only for $q_y \geq 0$. Explicit expressions for quantities involved in the producing the plots, along with the expressions of the functions stated in the legend, are given in Secs. 6.9.2 and 6.9.3 in the appendix.

[16]Instead of "magnetic excitation spectra", they will be referred to as "excitation spectra" throughout this section.

4.1 Non-altermagnetic limit of spin-flip susceptibilities

The leftmost panel of Fig. 8 display that when $m_1 \to m_2 = m$, referred to as the non-altermagnetic limit, we recover the expected excitation spectra for a non-interacting electron gas with a spin degenerate electronic band structure[11]. For non-interacting electrons which only undergo electron-hole excitations, the excitation spectra is referred to as the electron-hole continuum. The fact that this case is recovered strengthens the validity of the analytical results.

In the non-altermagnetic limit, the Fermi surface is a disk, and the inequalities determining the allowed excitation energies for $q_y \geq 0$ and $\omega \geq 0$ are given by

$$\max(0, \omega_{3,-}) \leq |\omega| \leq \omega_{3,+} \ , \ \lim_{m_1 \to m_2} \omega_{3,\pm} = \frac{(k_F \pm |q_y|)^2}{2m} - \frac{k_F^2}{2m},$$

where $k_F = \sqrt{2m\mu}$ is the Fermi wave vector. Physically, the maximum excitation energy ω_{1+}, corresponds to displacing an electron located at the Fermi surface radially outwards. Similarly, the minimum excitation energy $\omega_{1,-}$ corresponds to displacing an electron located at the Fermi surface radially inwards. Furthermore, for $q_y \leq 2k_F$, the magnitude of the minimum excitation energy tends to zero. This is because for any $q_y \leq 2k_F$, there exists some electron occupying a state at wave vector $\vec{k}$, such that $\vec{k} + \vec{q}$ is infinitesimally above the Fermi surface, meaning this process will involve infinitesimal energy transfer. For $q_y > 2k_F$, any electron will necessarily be displaced by a finite amount above the Fermi surface, meaning the process will involve finite energy transfer[11].

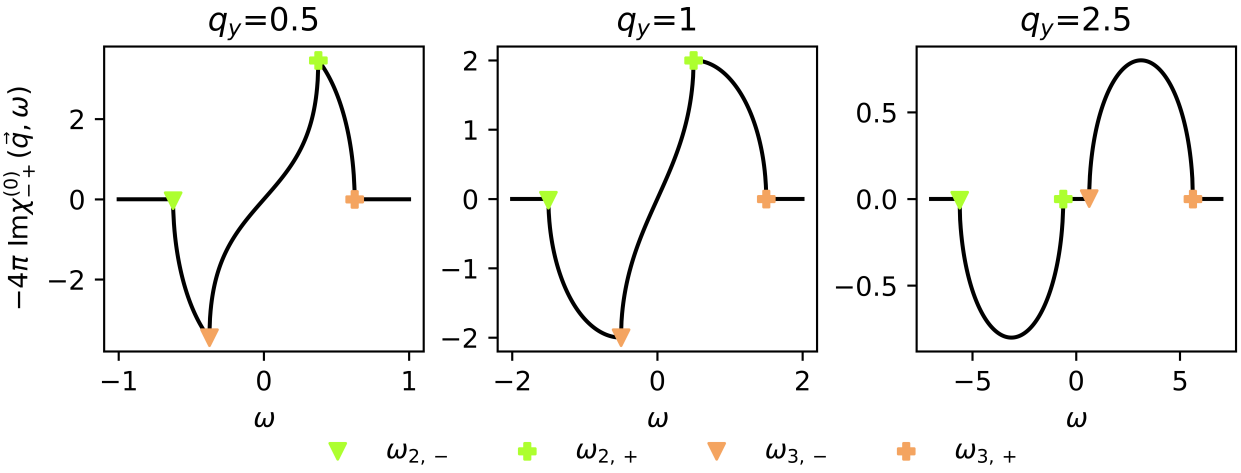

Figure 9: Cross sections taken from the imaginary part of $\chi^{(0)}_{-+}(\vec{q},\omega)$ for fixed values of q_y. Here, $m_1 \approx m_2 = 1$ and $k_F = 1$. The leftmost panel displays a "shark-fin" shape, a characteristic feature of the general non-interacting electron susceptibility (also known as the Lindhard function)[11].

Cross sections at fixed values of q_y in the non-altermagnetic limit, depicted in Fig. 9, display characteristic features for susceptibilities describing non-interacting electrons. For $q_y \leq 2k_F$,

sharp edges are observed as non-analytic features. For $q_y \geq 2k_F$, corners are observed at points where the spin-flip susceptibilities change from being zero to having finite values. Note that in the rightmost panel of Fig. 9, the positive and negative branches ($\chi^{(0)}_{-+}(\vec{q},\omega) > 0$ and $\chi^{(0)}_{-+}(\vec{q},\omega) < 0$ respectively) of excitation spectrum are symmetric with respect to their center in ω.

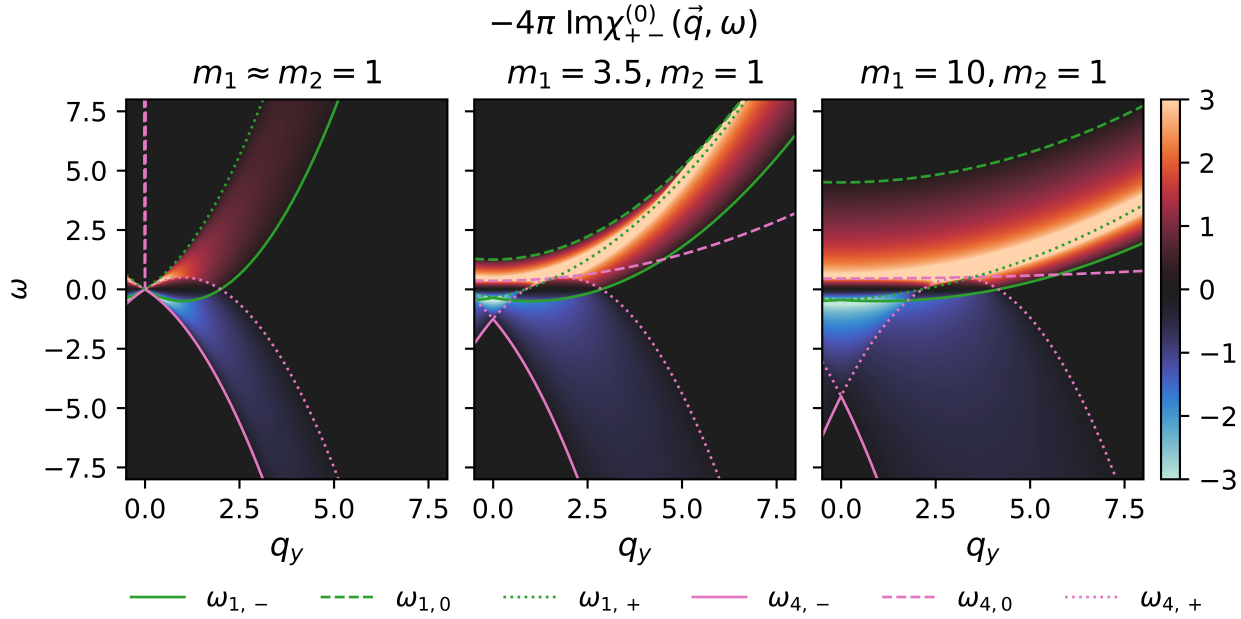

Figure 10: Imaginary part of $\chi^{(0)}_{+-}(\vec{q},\omega)$, displayed for different pairs of effective electron masses. As $\mathrm{Im}\chi^{(0)}_{+-}(\vec{q},\omega)$ is symmetric with respect to q_y, it is plotted only for $q_y \geq 0$. Explicit expressions for quantities involved in the producing the plots, along with the expressions of the functions stated in the legend are given in Secs. 6.9.1 and 6.9.4 in the appendix.

4.2 Altermagnetic regime of spin-flip susceptibilities

For the altermagnetic phase ($m_1 \neq m_2$), the spin-flip susceptibilities are symmetric with respect to q_y but are not anti-symmetric with respect to ω. It is evident from Figs. 8 and 10 that the spin-flip susceptibilities obey the symmetry relation given in Eq. (2.14). By these symmetry considerations, it will suffice to only discuss the results for the $\chi^{(0)}_{+-}(\vec{q},\omega)$ susceptibility.

The electronic band structure in the altermagnetic phase is spin polarized, leading to new features of excitation spectrum. Some immediate features displayed by the middle and rightmost panels in Fig. 10 are the broadening of the continuum as one of the effective electron masses is increased. This is a consequence of the Fermi wave vector $k_{F,1}$ being increased, which increases the amount of states inside the Fermi surface to participate in excitations. Furthermore, as the difference in effective mass increases, the region where the

positive and negative branches of the excitation spectrum overlap, decreases. Physically, this corresponds to the Fermi surfaces becoming more "steep" as the difference in effective electron mass grows. Hence there is a smaller overlap of the Fermi surfaces.

Another important feature of the altermagnetic spin-susceptibilities is the absence of a singularity at $q_y = 0$ in the middle and rightmost panels of Fig. 10. This is attributed to new possible excitation processes becoming available. Physical insight of these processes are obtained by examining the algebraic expressions for $\omega_{i,\pm}$ and $\omega_{i,0}$, where $i = 1, 4$[17]. Physically, $\omega_{1,+}$, given by Eq. (3.14), represents the excitation process of flipping the spin of an electron, and promoting it from a state located at the Fermi surface, to an unoccupied state above the Fermi surface, creating a hole in the process. Such excitations are known as single particle Stoner excitations[15]. Similarly, $\omega_{1,-}$ represents a single particle Stoner excitation, where the electron located at the Fermi surface is displaced radially inwards. Hence, the continuum of excitations observed at $q_y = 0$ in the altermagnetic spin-flip susceptibilities corresponds to electrons at different wave vectors $\vec{k}$ flipping their spins. This continuum appears as a consequence of breaking spin-degeneracy of the dispersion relation, as in the non-altermagnetic limit flipping spins has no impact on the electron energy, and hence is not a contributing excitation process.

For $q_y \leq k_{F,1} + k_{F,2}$ the magnitude of the minimum excitation energy tends to zero, indicated by the dark spots close to $\omega = 0$ in the middle and rightmost panels of Fig. 10. For $q_y \geq k_{F,1} + k_{F,2}$ the magnitude of the minimum excitation energy is finite. As excitation processes involve the flipping of spins, the smallest momentum transfer q_y which guarantees that any electron occupying some state at wave vector $\vec{k}$ is displaced finitely above the opposite spin Fermi surface, corresponds to the momentum transfer involved in exciting an electron located at the co-vertex of one of the Fermi surfaces such that it lands on the vertex of the opposite spin Fermi surface. For such an excitation process, $q_y = k_{F,1} + k_{F,2}$, and it necessarily involves finite energy transfer.

Of particular interest are the excitation processes described by $\omega_{i,0}$, displayed in Eq. (3.13) which diverges in the non-altermagnetic limit. Note, the nature of the $\omega_{1,0}$ and $\omega_{4,0}$ modes are fundamentally different, as $\omega_{1,0}$ persists as a possible excitation mode for any q_y, but $\omega_{4,0}$ modes only exist within a finite range of q_y values, as is depicted in the middle and rightmost panels of Fig. 10. By examining the algebraic structure of $\omega_{i,0}$ (see section Secs. 6.9.1 and 6.9.4 in the appendix) the physical origin of these modes are not trivially explained. It could be the case that their physical origin becomes more apparent if the susceptibilities were obtained for arbitrary $\vec{q}$-vectors. However, it has been argued that physical properties associated with a d-wave spin-split Fermi surface, which is realized by our model dispersion relation for the altermagnetic phase (Eq. (2.2)), can allow for unconventional electron excitation modes[4]. This could possibly explain the origin of the additional excitation modes appearing in the altermagnetic regime. Additional investigation into these modes is needed.

[17] In this section, $i = 1, 4$.

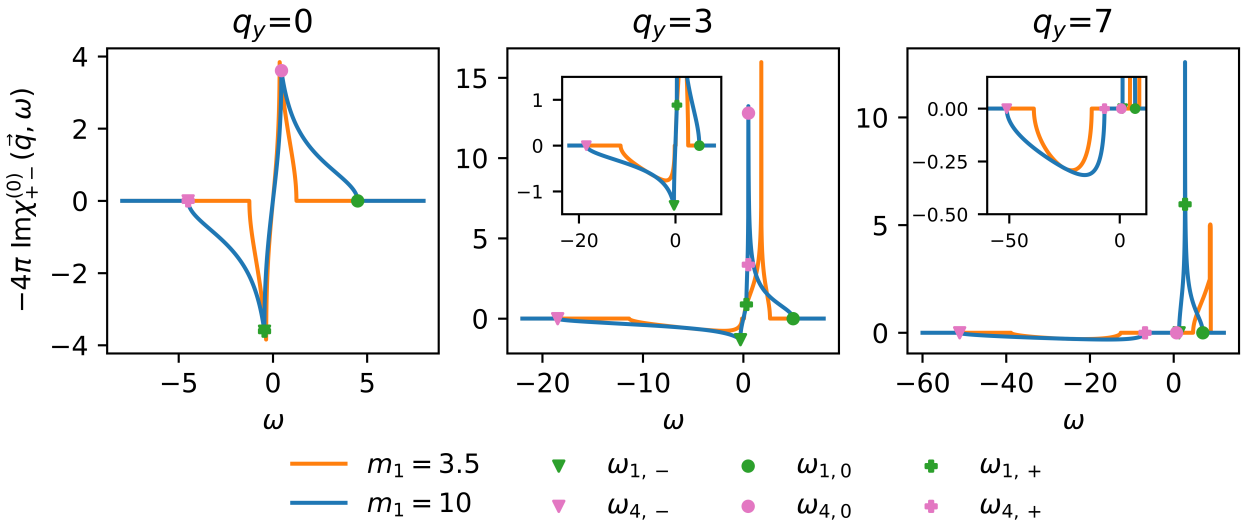

Figure 11: Cross sections taken from the imaginary part of $\chi^{(0)}_{+-}(\vec{q},\omega)$ for fixed values of q_y. The yellow lines display the cross sections for $m_1 = 3.5, m_2 = 1$, and the blue lines display the cross section for $m_1 = 10, m_2 = 1$. The marked points belong to the case when $m_1 = 10, m_2 = 1$, i.e. the blue lines. The insets of the middle and rightmost panels are enlarged images of the corresponding plots, used to display smaller features.

To further study the excitation modes, we consider cross sections at fixed values of q_y of the excitation spectra from the middle and rightmost panels in Fig. 10. These cross sections are depicted in Fig. 11. Apart from the resonance peaks, many features of the cross sections are reminiscent of those displayed in Fig. 9, like the nature of the non-analytic features (sharp edges and corners). Furthermore, what looks like the "inverted shark fin" is present in the leftmost and middle panel. Furthermore, the "half-circle" features, representing the negative branch of the excitation spectrum, are observable in the middle and right-most panels. This feature closely resembles those displayed in the rightmost panel of Fig. 9 for non-altermagnetic limit. However, a distinction is that half circles no longer appear symmetric in ω about their center. This symmetry breaking is exaggerated as the difference in the effective electron masses increases.

The resonance peaks observed in middle and rightmost panels of Figs. 10 and 11 corresponds to the discussed single particle Stoner excitation, when an electron located at the Fermi surface flips its spin and is displaced radially outwards. It should be noted that the mode $\omega_{4,0}$ is not in general a resonance mode, it happened to lie close to $\omega_{1,+}$ in the middle panel of Fig. 11. For sufficiently large values of ω and q_y[18], the $\omega_{1,+}$ mode converges to $\omega_{1,0}$. Notably, the resonance feature of the $\omega_{1,+}$ mode dissipates in this limit. The mathematical origin of dissipation stems from the convergence factor $e^{-\eta t}$, introduced in the temporal Fourier transform (see Eq. (2.4))[11].

[18]See Sec. 6.11 in the appendix for a plot displaying this feature.

The altermagnetic cross sections in Fig. 11 also allow us to study damping effects of long lived excitation modes. Specifically, for transverse spin susceptibilities, we can estimate the damping constant λ by[16]

$$\lambda \propto \lim_{\omega \to 0} \frac{\mathrm{Im}\chi^{(0)}_{+-}(\vec{q},\omega)}{\omega}.$$

Qualitative inspections of Fig. 11 shows that there is damping present when $q_y \leq k_{F,1} + k_{F,2}$. For $q_y > k_{F,1} + k_{F,2}$, the imaginary part of the spin-flip susceptibility is zero at $\omega = 0$, meaning there is no damping of long lived modes.

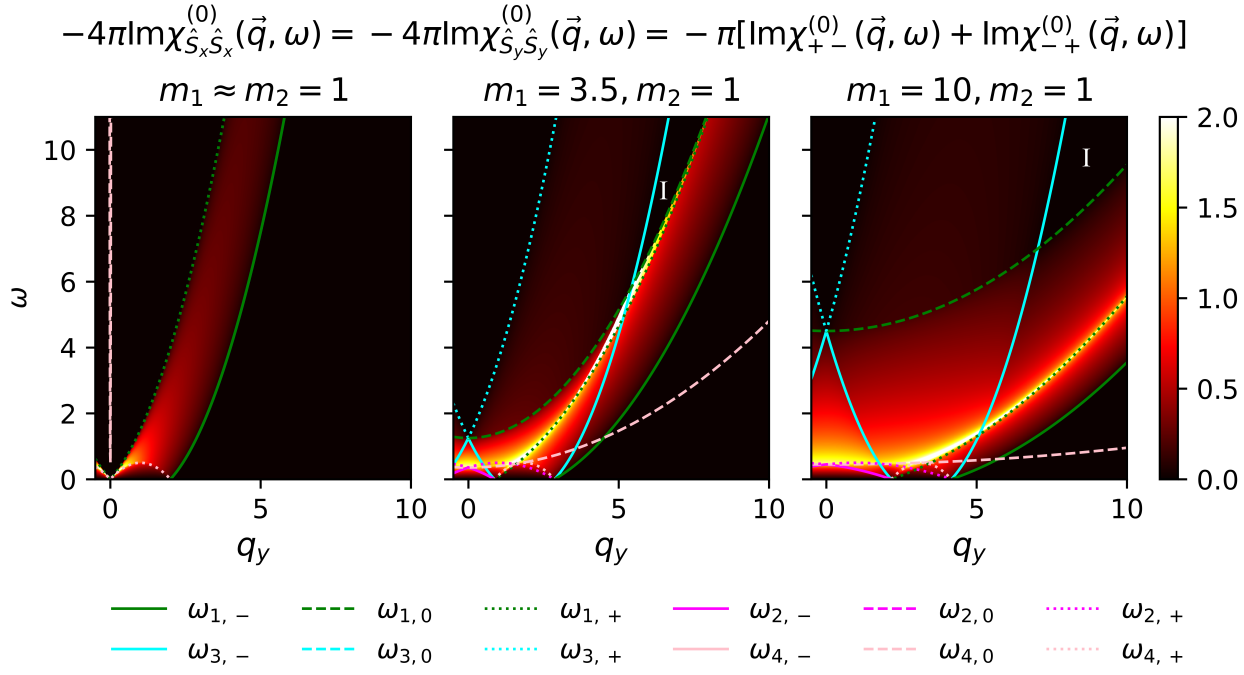

Figure 12: Imaginary part of spin-density susceptibility $\chi^{(0)}_{\hat{S}_x\hat{S}_x}(\vec{q},\omega)$, displayed for different pairs of effective electron masses. The region marked as I in the middle and rightmost panels determines the splitting of the spin-flip susceptibilities. By virtue of the spin-flip susceptibilities being symmetric with respect to q_y, and symmetry properties inherited by Eq. (2.14), it suffices to plot this quantity for $q_y \geq 0$ and $\omega \geq 0$.

4.3 Splitting of spin-flip susceptibilities

We are now in a position to predict the size of the splitting observed in the spin-flip susceptibilities. The middle and rightmost panels of Fig. 12 display a splitting in the spin-flip susceptibilities, denoted by the region marked as I. This is not present in the non-altermagnetic limit, as depicted by the leftmost panel in Fig. 12. The size of the splitting, Δ, predicted by our model can be analytically determined. For $q_y > 0$, the splitting is observable for $\omega > \omega_S$,

where

$$\omega_S = \frac{k_{F,1}^2(m_1 - m_2)}{2m_1 m_2} \left(\frac{m_1^2 + m_1 m_2 + m_2^2}{m_1^2 - m_1 m_2 - m_2^2} \right)^2,$$

and the magnitude of the splitting is given by

$$\Delta(\omega) = \sqrt{\left(\omega - \frac{k_{F,1}^2}{2m_2} + \frac{k_{F,1}^2}{2m_1} \right) \left(\frac{2(m_1^2 - m_2^2)}{m_1} \right)} - k_{F,1} - \sqrt{2m_2 \left(\omega + \frac{k_{F,1}^2}{2m_1} \right)}.$$

Clearly, this is a crude approximation, as by translational symmetry in solids, we expect back folding, meaning the joining of the branches at the boundaries of the Brillouin zone. This will not be observed for our model. Notably, this formula is not applicable in the non-altermagnetic limit, attributed to the divergence of $\omega_{1,0}$. Further aspects of the $\chi^{(0)}_{\hat{S}_x \hat{S}_x}(\vec{q}, \omega)$ susceptibility are not discussed, as many of the features stem from the spin-flip susceptibilities discussed in Sec. 4.2.

5 Conclusion and Outlook

In this thesis, we analytically obtained various spin susceptibilities for a simple minimal model of a non-interacting altermagnetic electron gas. Furthermore, we discussed the physical implications of the obtained susceptibilities by studying the corresponding excitation spectra. Lastly, we made a prediction of the size of the splitting between the spin flip susceptibilities in reciprocal space.

There is still a great deal of analytical considerations which can be done to improve the physical relevancy of the obtained susceptibilities. First, we ought to obtain an equation for the spin-flip susceptibilities for any arbitrary $\vec{q}$-vector. An identical method to that presented in this work may be used to obtain this result, and it was initially considered. In the case of arbitrary $\vec{q}$, the form of the integrand does not change much, however the integration boundaries become significantly more complicated and even somewhat tedious to solve for strong symbolic calculators like Mathematica. This is a consequence of non-zero q_x allowing for the hyperbola $\omega + \varepsilon_{\vec{k}\uparrow} - \varepsilon_{\vec{k}+\vec{q}\downarrow} = 0$ to be translated along both the k_x and k_y axes, whereas for $q_x = 0$, it can only be translated along the k_y-axis. This additional degree of freedom makes the equations describing the intersections between the Fermi surface and the hyperbola more intricate. We opted for $\vec{q} = (0, q_y)$ as an initial approach, as much of the underlying physics can still be obtained from this restriction.

Furthermore, to account for electron-electron interactions, we could incorporate the random-phase approximation into the susceptibilities. This would allow for the study of collective excitations such as plasmons and magnons in an interacting altermagnetic gas. Notably, no additional integration is required to implement the random phase approximation, only algebraic manipulations. It would also be of great interest to study the real part of the spin susceptibilities, which can be obtained by the Kramers-Kronig relations[11].

References

[1] Z. H. Stachurski, G. Wang, and X. Tan, "Chapter 6 - magnetic properties of amorphous metallic alloys," in *An Introduction to Metallic Glasses and Amorphous Metals*, pp. 157–192, Elsevier, 2021.

[2] S. G. Brush, "History of the Lenz-Ising model," *Rev. Mod. Phys.*, vol. 39, pp. 883–893, Oct 1967.

[3] N. F. Kharchenko, "On seven decades of antiferromagnetism," *Low Temperature Physics*, vol. 31, pp. 633–634, 08 2005.

[4] L. Šmejkal, J. Sinova, and T. Jungwirth, "Emerging research landscape of altermagnetism," *Phys. Rev. X*, vol. 12, p. 040501, Dec 2022.

[5] O. Fedchenko *et al.*, "Observation of time-reversal symmetry breaking in the band structure of altermagnetic ruo$_2$," *Science Advances*, vol. 10, no. 5, p. eadj4883, 2024.

[6] S. A. Wolf *et al.*, "Spintronics: A spin-based electronics vision for the future," *Science*, vol. 294, no. 5546, pp. 1488–1495, 2001.

[7] D. Chakraborty and A. M. Black-Schaffer, "Zero-field finite-momentum and field-induced superconductivity in altermagnets." arXiv preprint arXiv:2309.14427, 2024.

[8] T. A. Maier and S. Okamoto, "Weak-coupling theory of neutron scattering as a probe of altermagnetism," *Phys. Rev. B*, vol. 108, p. L100402, Sep 2023.

[9] P. Coleman, *Introduction to Many-Body Physics*. Cambridge University Press, 2015.

[10] *European Spallation Source, MIRACLES*. Accessed 2024-04-25, available at `https://europeanspallationsource.se/instruments/miracles`.

[11] G. Giuliani and G. Vignale, *Quantum Theory of the Electron Liquid*. Cambridge University Press, 2005.

[12] J. P. Sethna, *Statistical Mechanics: Entropy, Order Parameters and Complexity*. Great Clarendon Street, Oxford OX2 6DP: Oxford University Press, first edition ed., 2006.

[13] M. Sigrist, *Solid State Theory*. Lecture notes, 2014.

[14] K. F. Riley, M. P. Hobson, and S. J. Bence, *Mathematical Methods for Physics and Engineering: A Comprehensive Guide*. Cambridge University Press, 3 ed., 2006.

[15] C. Friedrich, E. Şaşıoğlu, M. Müller, A. Schindlmayr, and S. Blügel, *Spin Excitations in Solids from Many-Body Perturbation Theory*, pp. 259–301. Berlin, Heidelberg: Springer Berlin Heidelberg, 2014.

[16] K. Gilmore, *Precession damping in itinerant ferromagnets*. Phd thesis, Montana State University, November 2007.

6 Appendix

6.1 Spin-flip and rotation symmetry of the altermagnetic dispersion relation

We considered the dispersion relation

$$\varepsilon(\sigma, k_x, k_y) = \delta_{\sigma\uparrow}\left(\frac{k_x^2}{2m_1} + \frac{k_y^2}{2m_2}\right) + \delta_{\sigma\downarrow}\left(\frac{k_y^2}{2m_1} + \frac{k_x^2}{2m_2}\right),$$

We assume the effective mass tensors of the different hyperbolas are related by swapping the diagonal matrix elements, that is

$$[\mathcal{M}^{\uparrow}]^{-1} = \begin{bmatrix} \frac{1}{m_1} & 0 \\ 0 & \frac{1}{m_2} \end{bmatrix}, [\mathcal{M}^{\downarrow}]^{-1} = \begin{bmatrix} \frac{1}{m_2} & 0 \\ 0 & \frac{1}{m_1} \end{bmatrix}. \tag{6.1}$$

We wish to show the dispersion relation is invariant under combined spin-flip and 90°-rotation. The matrices which achieves these transformations are

$$\hat{S}_{sf} = \begin{bmatrix} 0 & 1 \\ 1 & 0 \end{bmatrix}, \quad \hat{R} = \begin{bmatrix} 0 & 1 \\ -1 & 0 \end{bmatrix},$$

where matrix $\hat{S}_{sf}$ acts only on the spin, and matrix $\hat{R}$ acts only on the wave vector. Clearly, $\hat{R}\vec{k} = (k_y, -k_x)$, and we can write $\hat{S}_{sf}\sigma = \bar{\sigma}$ where $\bar{\sigma}$ denotes the eigenvector of the z-spin matrix, different from σ. Noting that $\delta_{\sigma\uparrow} = \delta_{\bar{\sigma}\downarrow}$ and $\delta_{\sigma\downarrow} = \delta_{\bar{\sigma}\uparrow}$. Then,

$$\begin{aligned}
\varepsilon(\hat{S}_{sf}\sigma, \hat{R}\vec{k}) &= \varepsilon_{AM}(\bar{\sigma}, k_y, -k_x), \\
&= \delta_{\bar{\sigma}\uparrow}\left(\frac{k_y^2}{2m_1} + \frac{k_x^2}{2m_2}\right) + \delta_{\bar{\sigma}\downarrow}\left(\frac{k_x^2}{2m_1} + \frac{k_y^2}{2m_2}\right), \\
&= \delta_{\sigma\uparrow}\left(\frac{k_x^2}{2m_1} + \frac{k_y^2}{2m_2}\right) + \delta_{\sigma\downarrow}\left(\frac{k_y^2}{2m_1} + \frac{k_x^2}{2m_2}\right).
\end{aligned}$$

6.2 More on linear response theory

6.2.1 Susceptibilities for systems with translational symmetry

For systems with translational symmetry, the susceptibility depends on the relative distances only,

$$\chi_{AB}(\vec{r},\vec{r'},t) = \chi_{AB}(\vec{r}-\vec{r'},t).$$

The spatial Fourier transformed is computed through

$$\chi_{AB}(\vec{q},\vec{q'},t) \equiv \frac{1}{L^d}\int d\vec{r}e^{-i\vec{q}\cdot\vec{r}}\int d\vec{r'}e^{-i\vec{q'}\cdot\vec{r'}}\chi_{AB}(\vec{r},\vec{r'},t),$$

and introducing the change of variables

$$\vec{r} = \vec{R}+\frac{\vec{\rho}}{2}\ ,\ \vec{r'} = \vec{R}-\frac{\vec{\rho}}{2}\ ,\ d\vec{r}d\vec{r'} = d\vec{R}d\vec{\rho},$$

yields

$$\begin{aligned}\chi_{AB}(\vec{q},\vec{q'},t) &= \frac{1}{L^d}\int d\vec{R}e^{-i\vec{R}\cdot(\vec{q}-(-\vec{q'}))}\int d\vec{\rho}e^{-i\frac{\vec{\rho}}{2}\cdot(\vec{q}-\vec{q'})}\chi_{AB}(\vec{\rho},t),\\ &= \delta_{\vec{q},-\vec{q'}}\int d\vec{\rho}e^{-i\vec{\rho}\cdot\vec{q}}\chi_{AB}(\vec{\rho},t),\\ &= \delta_{\vec{q},-\vec{q'}}\chi_{AB}(\vec{q},t),\end{aligned}$$

where we used that

$$\int e^{-i\vec{r}\cdot(\vec{q}-\vec{q'})}d\vec{r} = L^d\delta_{\vec{q},\vec{q'}}.$$

Finally, for systems with translational symmetry,

$$\chi_{AB}(\vec{q},t) = \chi_{AB}(\vec{q},-\vec{q},t). \tag{6.2}$$

6.2.2 Two ways to calculate the Fourier transform of the susceptibility

In general, the spacial dependence of the susceptibility enters through the operators (see Eq. (2.3)), which allows us to write $\chi_{AB}(\vec{r},\vec{r'},t) = \chi_{A(\vec{r})B(\vec{r'})}(t)$. Hence, we can perform a Fourier transform on the individual operators before computing the susceptibility, which allows us to write

$$\chi_{AB}(\vec{q},\vec{q'},\omega) = \frac{1}{L^d}\chi_{A_{\vec{q}}B_{\vec{q'}}}(\omega). \tag{6.3}$$

Here, $\hat{A}_{\vec{q}}$ denotes the spatial Fourier transform of operator $\hat{A}$. In particular, for systems with translational symmetry, we showed that the spacial Fourier transform depends on a single $\vec{q}$, and is given by Eq. (6.2). Combining Eq. (6.3) and (6.2), we obtain the known literature result [11]

$$\chi_{AB}(\vec{q},\omega) = \frac{1}{L^d}\chi_{A_{\vec{q}}B_{-\vec{q}}}(\omega), \tag{6.4}$$

which will be used to compute relevant susceptibilities.

6.3 More on linear response theory for independent electrons

Applying Eq. (2.5) on Eq. (2.3), the susceptibility expressed in terms of single particle operators acting on independent electrons is given by

$$\chi^{(0)}_{AB}(\vec{r},\vec{r'},t) = -i\Theta(t)\sum_{\alpha\beta\gamma\delta} A_{\alpha\beta}B_{\gamma\delta}e^{-i(\varepsilon_\alpha-\varepsilon_\beta)t}\left\langle\left[\hat{c}^\dagger_\alpha\hat{c}_\beta,\hat{c}^\dagger_\gamma\hat{c}_\delta\right]\right\rangle_0,$$

where the spatial dependence is accounted for in the matrix elements $A_{\alpha,\beta}, B_{\gamma,\delta}$. Evaluating the commutator[19] and computing the Fourier transform in space and time using Eq. (6.4) (assuming translational symmetry) gives

$$\chi^{(0)}_{AB}(\vec{q},\omega) = \frac{1}{L^d}\sum_{\alpha\beta}\frac{n_\alpha - n_\beta}{\omega+\varepsilon_\alpha-\varepsilon_\beta+i\eta}\left(A_{\vec{q}}\right)_{\alpha\beta}\left(B_{-\vec{q}}\right)_{\beta\alpha}.$$

Furthermore, we can decompose the susceptibility into a real and imaginary part by the use of

$$\lim_{\eta\to 0}\frac{1}{\omega-t\pm i\eta} = \mathcal{P}\frac{1}{\omega-t}\mp i\pi\delta(\omega-t),$$

where the $\mathcal{P}$ denotes the Cauchy-Hadamard principle value distribution [11]. From this, we may write the imaginary part of the general, independent electron susceptibility as

$$\mathrm{Im}\chi^{(0)}_{AB}(\vec{q},\omega) = -\frac{\pi}{L^d}\sum_{\alpha\beta}\left(n_\alpha-n_\beta\right)\delta(\omega+\varepsilon_\alpha-\varepsilon_\beta)\left(A_{\vec{q}}\right)_{\alpha\beta}\left(B_{-\vec{q}}\right)_{\beta\alpha}.$$

6.4 Relevant commutators and anti-commutators

Fermionic creation and annihilation operators obey the anti-commutators

$$\left\{\hat{c}^\dagger_\alpha,\hat{c}^\dagger_\beta\right\} = \{\hat{c}_\alpha,\hat{c}_\beta\} = 0, \quad \left\{\hat{c}_\alpha,\hat{c}^\dagger_\beta\right\} = \delta_{\alpha\beta}.$$

Then, using $[A,BC] = [A,B]\,C + B\,[A,C]$ and $[AB,C] = A\,\{B,C\} - \{A,C\}\,B$,

$$\begin{aligned}
\left[\hat{c}^\dagger_\alpha\hat{c}_\beta,\hat{c}^\dagger_\gamma\hat{c}_\delta\right] &= \left[\hat{c}^\dagger_\alpha\hat{c}_\beta,\hat{c}^\dagger_\gamma\right]\hat{c}_\delta + \hat{c}^\dagger_\gamma\left[\hat{c}^\dagger_\alpha\hat{c}_\beta,\hat{c}_\delta\right]\\
&= \hat{c}^\dagger_\alpha\left\{\hat{c}_\beta,\hat{c}^\dagger_\gamma\right\}\hat{c}_\delta - \left\{\hat{c}^\dagger_\alpha,\hat{c}^\dagger_\gamma\right\}\hat{c}_\beta\hat{c}_\delta + \hat{c}^\dagger_\gamma\hat{c}^\dagger_\alpha\left\{\hat{c}_\beta,\hat{c}_\delta\right\} - \hat{c}^\dagger_\gamma\left\{\hat{c}^\dagger_\alpha,\hat{c}_\delta\right\}\hat{c}_\beta,\\
&= \hat{c}^\dagger_\alpha\hat{c}_\delta\delta_{\beta\gamma} - \hat{c}^\dagger_\gamma\hat{c}_\beta\delta_{\alpha\delta},\\
&= \delta_{\beta\gamma}\delta_{\alpha\delta}\left(\hat{c}^\dagger_\alpha\hat{c}_\alpha - \hat{c}^\dagger_\beta\hat{c}_\beta\right),\\
&= \delta_{\beta\gamma}\delta_{\alpha\delta}\left(\hat{N}_\alpha - \hat{N}_\beta\right),
\end{aligned}$$

where $\hat{N}_\alpha$ is the number operator, giving the number of particles in state α. Taking the expectation value of the operators for independent electrons $\left(\hat{H}_0 = \sum_\alpha \varepsilon_\alpha\hat{c}^\dagger_\alpha\hat{c}_\alpha\right)$,

$$\left\langle\left[\hat{c}^\dagger_\alpha\hat{c}_\beta,\hat{c}^\dagger_\gamma\hat{c}_\delta\right]\right\rangle_0 = \delta_{\beta\gamma}\delta_{\alpha\delta}\left(n_\alpha-n_\beta\right),$$

where $n_\alpha = \frac{1}{e^{\beta(\varepsilon_\alpha-\mu)+1}}$ is the usual Fermi-Dirac distribution for electrons in state α with associated energy ε_α.

[19] See appendix 6.4

6.5 Second quantization of spin density operators

We wish to obtain a general formula for second quantization of Fourier transformed of spin densities. That is, obtaining a second quantization of

$$\hat{S}_{\beta,\vec{q}} = \sum_i \hat{\vec{S}}_{\beta,i} e^{-i\vec{q}\cdot\vec{r}_i}.$$

for $\beta = x, y, z, +, -$. Using the single particle eigenstates $\frac{1}{\sqrt{L^d}} e^{i\vec{k}\cdot\vec{r}}\delta_{s\sigma}$,

$$\begin{aligned}\hat{S}_{\beta,\vec{q}} &= \sum_{\vec{k}\sigma,\vec{k}'\sigma'} \langle \vec{k}\sigma|\hat{S}_{\beta,\vec{q}}|\vec{k}'\sigma'\rangle \hat{c}^\dagger_{\vec{k}\sigma}\hat{c}_{\vec{k}'\sigma'}, \\ &= \sum_{\vec{k}\sigma,\vec{k}'\sigma'} \langle \vec{k}|e^{-i\vec{q}\cdot\vec{r}}|\vec{k}'\rangle\langle\sigma|\hat{S}_\beta|\sigma'\rangle \hat{c}^\dagger_{\vec{k}\sigma}\hat{c}_{\vec{k}'\sigma'},\end{aligned}$$

where

$$\left\langle \vec{k}\left|e^{-i\vec{q}\cdot\vec{r}}\right|\vec{k}'\right\rangle = \frac{1}{L^d}\int d\vec{r} e^{-i\vec{r}\cdot\left(\vec{k}+\vec{q}-\vec{k}'\right)} = \delta_{\vec{k}',\vec{k}+\vec{q}} = \delta_{\vec{k},\vec{k}'-\vec{q}},$$

is a reoccurring matrix element. Then,

$$\hat{S}_{\beta,\vec{q}} = \sum_{k\sigma\sigma'} \langle\sigma|\hat{S}_\beta|\sigma'\rangle \hat{c}^\dagger_{\vec{k}-\vec{q}\sigma}\hat{c}_{\vec{k}\sigma'}.$$

Then, the second quantization of the considered spin density operators are given by

$$\hat{S}_{\vec{q},+} = \sum_{\vec{k}} \hat{c}^\dagger_{\vec{k}-\vec{q}\uparrow}\hat{c}_{\vec{k}\downarrow}\ ,\ \hat{S}_{\vec{q},-} = \sum_{\vec{k}} \hat{c}^\dagger_{\vec{k}-\vec{q}\downarrow}\hat{c}_{\vec{k}\uparrow},$$

$$\begin{aligned}\hat{S}_{\vec{q},x} &= \frac{1}{2}\sum_{\vec{k}} \left(\hat{c}^\dagger_{\vec{k}-\vec{q}\uparrow}\hat{c}_{\vec{k}\downarrow} + \hat{c}^\dagger_{\vec{k}-\vec{q}\downarrow}\hat{c}_{\vec{k}\uparrow}\right), \\ \hat{S}_{\vec{q},y} &= \frac{1}{2i}\sum_{\vec{k}} \left(\hat{c}^\dagger_{\vec{k}-\vec{q}\uparrow}\hat{c}_{\vec{k}\downarrow} - \hat{c}^\dagger_{\vec{k}-\vec{q}\downarrow}\hat{c}_{\vec{k}\uparrow}\right), \\ \hat{S}_{\vec{q},z} &= \frac{1}{2}\sum_{\vec{k}} \left(\hat{c}^\dagger_{\vec{k}-\vec{q}\uparrow}\hat{c}_{\vec{k}\uparrow} - \hat{c}^\dagger_{\vec{k}-\vec{q}\downarrow}\hat{c}_{\vec{k}\downarrow}\right).\end{aligned}$$

6.6 Explicit determination of spin susceptibilities

The spin operators are given by $\hat{S}_i = \frac{1}{2}\hat{\sigma}_i$ for $i = x, y, z$, and $\hat{\sigma}$ represents a Pauli spin matrix

$$\hat{\sigma}_x = \begin{pmatrix} 0 & 1 \\ 1 & 0 \end{pmatrix} \quad , \quad \hat{\sigma}_y = \begin{pmatrix} 0 & -i \\ i & 0 \end{pmatrix} \quad , \quad \hat{\sigma}_z = \begin{pmatrix} 1 & 0 \\ 0 & -1 \end{pmatrix}.$$

As $\hat{S}_+ = \hat{S}_x + i\hat{S}_y$ and $\hat{S}_- = \hat{S}_x - i\hat{S}_y$, we obtain operators

$$\hat{S}_+ = \begin{pmatrix} 0 & 1 \\ 0 & 0 \end{pmatrix} \quad , \quad \hat{S}_- = \begin{pmatrix} 0 & 0 \\ 1 & 0 \end{pmatrix}.$$

Note how $\hat{S}_+|\downarrow\rangle = |\uparrow\rangle$ and $\hat{S}_-|\uparrow\rangle = |\downarrow\rangle$.

To calculate susceptibilities $\chi^{(0)}_{\hat{S}_z\hat{S}_z}(\vec{q},\omega), \chi^{(0)}_{+-}(\vec{q},\omega)$ and $\chi^{(0)}_{-+}(\vec{q},\omega)$ requires the determination of matrix elements $(A_{\vec{q}})_{\vec{k}\sigma,\vec{k}'\sigma'}\,(B_{-\vec{q}})_{\vec{k}'\sigma',\vec{k}\sigma}$. Beginning with the $\hat{S}_{z,\vec{q}}$ operator, the relevant matrix element needed is (see Eq. (2.5))

$$\begin{aligned}(S_{z,\vec{q}})_{\vec{k}\sigma,\vec{k}'\sigma'} &= \left\langle \vec{k}\sigma \left| \hat{S}_z e^{-i\vec{q}\cdot\vec{r}} \right| \vec{k}'\sigma' \right\rangle, \\ &= \frac{1}{2}\left\langle \sigma \left| \hat{\sigma}_z \right| \sigma' \right\rangle \left\langle \vec{k} \left| e^{-i\vec{q}\cdot\vec{r}} \right| \vec{k}' \right\rangle.\end{aligned}$$

Here,

$$\left\langle \vec{k} \left| e^{-i\vec{q}\cdot\vec{r}} \right| \vec{k}' \right\rangle = \frac{1}{L^d}\int d\vec{r} e^{-i\vec{r}\cdot\left(\vec{k}+\vec{q}-\vec{k}'\right)} = \delta_{\vec{k}',\vec{k}+\vec{q}} = \delta_{\vec{k},\vec{k}'-\vec{q}},$$

is a reoccurring matrix element. Taking the conjugate, $\left\langle \vec{k}' \left| e^{i\vec{q}\cdot\vec{r}} \right| \vec{k} \right\rangle = \delta_{\vec{k}',\vec{k}+\vec{q}}$. Then, the susceptibility $\chi^{(0)}_{\hat{S}_z\hat{S}_z}(\vec{q},\omega)$ is

$$\chi^{(0)}_{\hat{S}_z\hat{S}_z}(\vec{q},\omega) = \frac{1}{4L^d}\sum_{\vec{k}\sigma\vec{k}'\sigma'} \frac{n_{\vec{k}\sigma} - n_{\vec{k}'\sigma'}}{\omega + \varepsilon_{\vec{k}\sigma} - \varepsilon_{\vec{k}'\sigma'} + i\eta} \left\langle \sigma \left| \hat{\sigma}_z \right| \sigma' \right\rangle \left\langle \vec{k} \left| e^{-i\vec{q}\cdot\vec{r}} \right| \vec{k}' \right\rangle \left\langle \sigma' \left| \hat{\sigma}_z \right| \sigma \right\rangle \left\langle \vec{k}' \left| e^{i\vec{q}\cdot\vec{r}} \right| \vec{k} \right\rangle,$$

$$\begin{aligned}&= \frac{1}{4L^d}\sum_{\vec{k}\sigma\sigma'} \frac{n_{\vec{k}\sigma} - n_{\vec{k}+\vec{q}\sigma'}}{\omega + \varepsilon_{\vec{k}\sigma} - \varepsilon_{\vec{k}+\vec{q}\sigma'} + i\eta} \left\langle \sigma \left| \hat{\sigma}_z \right| \sigma' \right\rangle \left\langle \sigma' \left| \hat{\sigma}_z \right| \sigma \right\rangle, \\ &= \frac{1}{4L^d}\sum_{\vec{k}\sigma} \frac{n_{\vec{k}\sigma} - n_{\vec{k}+\vec{q}\sigma}}{\omega + \varepsilon_{\vec{k}\sigma} - \varepsilon_{\vec{k}+\vec{q}\sigma} + i\eta}.\end{aligned}$$

For susceptibilities $\chi^{(0)}_{+-}(\vec{q},\omega)$ and $\chi^{(0)}_{-+}(\vec{q},\omega)$,

$$\begin{aligned}(S_{+,\vec{q}})_{\vec{k}\sigma,\vec{k}'\sigma'} &= \left\langle \vec{k}\sigma \left| \hat{S}_+ e^{-i\vec{q}\cdot\vec{r}} \right| \vec{k}'\sigma' \right\rangle, \\ &= \left\langle \sigma \left| \hat{S}_+ \right| \sigma' \right\rangle \delta_{\vec{k}',\vec{k}+\vec{q}}, \\ (S_{-,\vec{q}})_{\vec{k}\sigma,\vec{k}'\sigma'} &= \left\langle \sigma \left| \hat{S}_- \right| \sigma' \right\rangle \delta_{\vec{k}',\vec{k}+\vec{q}}.\end{aligned}$$

Then,

$$\begin{aligned}\chi^{(0)}_{+-}(\vec{q},\omega) &= \frac{1}{L^d}\sum_{\vec{k}\sigma\sigma'}\frac{n_{\vec{k}\sigma}-n_{\vec{k}+\vec{q}\sigma'}}{\omega+\varepsilon_{\vec{k}\sigma}-\varepsilon_{\vec{k}+\vec{q}\sigma'}+i\eta}\left\langle\sigma\left|\hat{S}_+\right|\sigma'\right\rangle\left\langle\sigma'\left|\hat{S}_-\right|\sigma\right\rangle,\\ &= \frac{1}{L^d}\sum_{\vec{k}}\frac{n_{\vec{k}\uparrow}-n_{\vec{k}+\vec{q}\downarrow}}{\omega+\varepsilon_{\vec{k}\uparrow}-\varepsilon_{\vec{k}+\vec{q}\downarrow}+i\eta}.\end{aligned}$$

Similarly for $\chi^{(0)}_{-+}(\vec{q},\omega)$

$$\chi^{(0)}_{-+}(\vec{q},\omega) = \frac{1}{L^d}\sum_{\vec{k}}\frac{n_{\vec{k}\downarrow}-n_{\vec{k}+\vec{q}\uparrow}}{\omega+\varepsilon_{\vec{k}\downarrow}-\varepsilon_{\vec{k}+\vec{q}\uparrow}+i\eta}.$$

For $\chi^{(0)}_{\hat{S}_x\hat{S}_x}(\vec{q},\omega)$,

$$\begin{aligned}\chi^{(0)}_{\hat{S}_x\hat{S}_x}(\vec{q},\omega) &= \frac{1}{4L^d}\sum_{\vec{k}\sigma\sigma'}\frac{n_{\vec{k}\sigma}-n_{\vec{k}+\vec{q}\sigma'}}{\omega+\varepsilon_{\vec{k}\sigma}-\varepsilon_{\vec{k}+\vec{q}\sigma'}+i\eta}\left\langle\sigma\left|\hat{\sigma}_x\right|\sigma'\right\rangle\left\langle\sigma'\left|\hat{\sigma}_x\right|\sigma\right\rangle,\\ &= \frac{1}{4L^d}\sum_{\vec{k}}\left(\frac{n_{\vec{k}\uparrow}-n_{\vec{k}+\vec{q}\downarrow}}{\omega+\varepsilon_{\vec{k}\uparrow}-\varepsilon_{\vec{k}+\vec{q}\downarrow}+i\eta}+\frac{n_{\vec{k}\downarrow}-n_{\vec{k}+\vec{q}\uparrow}}{\omega+\varepsilon_{\vec{k}\downarrow}-\varepsilon_{\vec{k}+\vec{q}\uparrow}+i\eta}\right),\end{aligned}$$

and it is easily verified that $\chi^{(0)}_{\hat{S}_x\hat{S}_x}(\vec{q},\omega)=\chi^{(0)}_{\hat{S}_y\hat{S}_y}(\vec{q},\omega)$. For $\chi^{(0)}_{\hat{S}_x\hat{S}_y}(\vec{q},\omega)$,

$$\begin{aligned}\chi^{(0)}_{\hat{S}_x\hat{S}_y}(\vec{q},\omega) &= \frac{1}{4L^d}\sum_{\vec{k}\sigma\sigma'}\frac{n_{\vec{k}\sigma}-n_{\vec{k}+\vec{q}\sigma'}}{\omega+\varepsilon_{\vec{k}\sigma}-\varepsilon_{\vec{k}+\vec{q}\sigma'}+i\eta}\left\langle\sigma\left|\hat{\sigma}_x\right|\sigma'\right\rangle\left\langle\sigma'\left|\hat{\sigma}_y\right|\sigma\right\rangle,\\ &= \frac{i}{4L^d}\sum_{\vec{k}}\left(\frac{n_{\vec{k}\uparrow}-n_{\vec{k}+\vec{q}\downarrow}}{\omega+\varepsilon_{\vec{k}\uparrow}-\varepsilon_{\vec{k}+\vec{q}\downarrow}+i\eta}-\frac{n_{\vec{k}\downarrow}-n_{\vec{k}+\vec{q}\uparrow}}{\omega+\varepsilon_{\vec{k}\downarrow}-\varepsilon_{\vec{k}+\vec{q}\uparrow}+i\eta}\right).\end{aligned}$$

We may then establish the relations

$$\begin{aligned}\chi^{(0)}_{\hat{S}_x\hat{S}_x}(\vec{q},\omega) &= \frac{1}{4}\left(\chi^{(0)}_{+-}(\vec{q},\omega)+\chi^{(0)}_{-+}(\vec{q},\omega)\right),\\ \chi^{(0)}_{\hat{S}_x\hat{S}_y}(\vec{q},\omega) &= \frac{i}{4}\left(\chi^{(0)}_{+-}(\vec{q},\omega)-\chi^{(0)}_{-+}(\vec{q},\omega)\right).\end{aligned}$$

6.7 Casting the sums in the susceptibilities into integrals

As a guiding example, consider the susceptibility

$$\chi^{(0)}_{+-}(\vec{q},\omega) = \frac{1}{L^d}\sum_{\vec{k}} \frac{n_{\vec{k}\uparrow} - n_{\vec{k}+\vec{q}\downarrow}}{\omega + \varepsilon_{\vec{k}\uparrow} - \varepsilon_{\vec{k}+\vec{q}\downarrow} + i\eta}.$$

Casting the sum over $\vec{k}$ into an integral according to $\sum_k \to \frac{L^d}{(2\pi)^d}\int d\vec{k}$ allows us to write

$$\begin{aligned}\chi^{(0)}_{+-}(\vec{q},\omega) &= \frac{1}{(2\pi)^d}\int_{-\infty}^{\infty} \frac{n_{\vec{k}\uparrow} - n_{\vec{k}+\vec{q}\downarrow}}{\omega + \varepsilon_{\vec{k}\uparrow} - \varepsilon_{\vec{k}+\vec{q}\downarrow} + i\eta}\, d\vec{k}, \\ &= \frac{1}{(2\pi)^d}\left[\int_{-\infty}^{\infty} \frac{n_{\vec{k}\uparrow}}{\omega + \varepsilon_{\vec{k}\uparrow} - \varepsilon_{\vec{k}+\vec{q}\downarrow} + i\eta}\, d\vec{k} - \int_{-\infty}^{\infty} \frac{n_{\vec{k}+\vec{q}\downarrow}}{\omega + \varepsilon_{\vec{k}\uparrow} - \varepsilon_{\vec{k}+\vec{q}\downarrow} + i\eta}\, d\vec{k}\right].\end{aligned}$$

Letting $\vec{k} \to \vec{k} - \vec{q}$ in the second integral,

$$\chi^{(0)}_{+-}(\vec{q},\omega) = \frac{1}{(2\pi)^d}\left[\int_{-\infty}^{\infty} \frac{n_{\vec{k}\uparrow}}{\omega + \varepsilon_{\vec{k}\uparrow} - \varepsilon_{\vec{k}+\vec{q}\downarrow} + i\eta}\, d\vec{k} - \int_{-\infty}^{\infty} \frac{n_{\vec{k}\downarrow}}{\omega + \varepsilon_{\vec{k}-\vec{q}\uparrow} - \varepsilon_{\vec{k}\downarrow} + i\eta}\, d\vec{k}\right].$$

Assuming $T = 0$, $n_{\vec{k}\uparrow} = \Theta(\vec{k}_{F\uparrow} - \vec{k})$ and $n_{\vec{k}\downarrow} = \Theta(\vec{k}_{F\downarrow} - \vec{k})$, which determines the integration region. Then, we write

$$\chi^{(0)}_{+-}(\vec{q},\omega) = \frac{1}{(2\pi)^d}\left[\int_{n_{\vec{k}\uparrow}=1} \frac{1}{\omega + \varepsilon_{\vec{k}\uparrow} - \varepsilon_{\vec{k}+\vec{q}\downarrow} + i\eta}\, d\vec{k} - \int_{n_{\vec{k}\downarrow}=1} \frac{1}{\omega + \varepsilon_{\vec{k}-\vec{q}\uparrow} - \varepsilon_{\vec{k}\downarrow} + i\eta}\, d\vec{k}\right].$$

As the limit $\eta \to 0$ will eventually be considered, we may use the identity

$$\lim_{\eta\to 0} \frac{1}{\omega - t \pm i\eta} = \mathcal{P}\frac{1}{\omega - t} \mp i\pi\delta(\omega - t),$$

where the $\mathcal{P}$ denotes the Cauchy-Hadamard principle value distribution [11]. Then, we obtain

$$\mathrm{Im}\chi^{(0)}_{+-}(\vec{q},\omega) = -\frac{\pi}{(2\pi)^d}\left[\int_{n_{\vec{k}\uparrow}=1} d\vec{k}\,\delta(\omega + \varepsilon_{\vec{k}\uparrow} - \varepsilon_{\vec{k}+\vec{q}\downarrow}) - \int_{n_{\vec{k}\downarrow}=1} d\vec{k}\,\delta(\omega + \varepsilon_{\vec{k}-\vec{q}\uparrow} - \varepsilon_{\vec{k}\downarrow})\right].$$

6.8 Evaluating the indefinite integral $\int \frac{1}{\sqrt{(x-a)^2+b}}dx$

Integrals of the form

$$\int \frac{1}{\sqrt{(x-a)^2+b}}dx,$$

appear in many places throughout the thesis, meaning an explicit treatment of the integral is called for. Assuming $b > 0$, we may let $x = \sqrt{b}t + a$, to obtain

$$\int \frac{\sqrt{b}}{\sqrt{bt^2+b}}dt = \int \frac{1}{\sqrt{1+t^2}}dt.$$

Letting $t = \tan\theta$,

$$\begin{aligned}\int \frac{1}{\sqrt{1+t^2}}dt &= \int \frac{\sec^2\theta}{\sqrt{1+\tan^2\theta}}d\theta,\\ &= \int \frac{\sec\theta(\tan\theta+\sec\theta)}{(\tan\theta+\sec\theta)}d\theta.\end{aligned}$$

Letting $u = \tan\theta + \sec\theta$, $du = \tan\theta\sec\theta + \sec^2\theta d\theta$, meaning

$$\begin{aligned}\int \sec\theta d\theta &= \int \frac{1}{u}du,\\ &= \ln(\tan\theta+\sec\theta) + D,\\ &= \ln\left(t+\sqrt{1+t^2}\right) + D,\\ &= \ln\left(\frac{x-a}{\sqrt{b}} + \sqrt{1+\left(\frac{x-a}{\sqrt{b}}\right)^2}\right) + D,\\ &= \ln\left((x-a)+\sqrt{b+(x-a)^2}\right).\end{aligned}$$

6.9 Results from spin-flip susceptibility integrals

Here, we state the analytical results from all of the double integrals involved in calculating the spin-flip susceptibilities. To make physical connections more concrete, we introduce the variables $k_{F,1} = \sqrt{2m_1\mu}$ and $k_{F,2} = \sqrt{2m_2\mu}$. Geometrically, these quantities correspond to the lengths of the axes of the ellipsoidal Fermi surfaces.

For brevity of notation, we split the results of the integrals into cases depending on the orientation of the Fermi surface, and the sign of the momentum transfer $\vec{q}$. For instance, the case $n_{\vec{k}\uparrow} = 1, \varepsilon_{\vec{k}+\vec{q}\downarrow}$ would correspond to the results obtained in Sec. 3.2.1.

6.9.1 Case 1, $n_{\vec{k}\uparrow} = 1$, $\varepsilon_{\vec{k}+\vec{q}\downarrow}$

$$\int_{n_{\vec{k}\uparrow}=1, K_- \leq 0} d\vec{k}\delta(\omega + \varepsilon_{\vec{k}\uparrow} - \varepsilon_{\vec{k}+\vec{q}\downarrow}) = M\log\left(\frac{\sqrt{k_{1,+,-}^2 - P_-^2} + k_{1,+,-}}{\sqrt{k_{1,-,-}^2 - P_-^2} + k_{1,-,-}}\right) + M\log\left(\frac{\sqrt{k_{1,+,+}^2 - P_-^2} + k_{1,+,+}}{\sqrt{k_{1,-,+}^2 - P_-^2} + k_{1,-,+}}\right),$$

$$\int_{n_{\vec{k}\uparrow}=1, K_- \geq 0} d\vec{k}\ \delta(\omega + \varepsilon_{\vec{k}\uparrow} - \varepsilon_{\vec{k}+\vec{q}\downarrow}) = 2M\log\left(\frac{\sqrt{P_-^2 + (k_{1,+} - Y_2)^2} + (k_{1,+} - Y_2)}{\sqrt{P_-^2 + (k_{1,-} - Y_2)^2} + (k_{1,-} - Y_2)}\right),$$

$$k_{1,\pm} = \frac{Y_2(M-R) \pm \sqrt{-4K_-M^2(M-R) + 8\mu M^2 R - Y_2^2(M^2 - R^2)}}{2M},$$
$$k_{1,\pm,\pm} = \pm\sqrt{\frac{(M+R)[|Y_2|\,(2Mk_{1,\pm} - Y_2(M-R)) + 2K_-M^2 + Y_2^2R] + 4\mu M^2 R}{2M^2}},$$

$$\omega_{1,0} = \frac{k_{F,1}^2}{2m_2} + \frac{q_y^2}{2m_2}\left(\frac{m_1m_2}{m_1^2 - m_2^2}\right) - \frac{k_{F,1}^2}{2m_1},$$
$$\omega_{1,\pm} = \frac{(k_{F,2} \pm |q_y|)^2}{2m_1} - \frac{k_{F,2}^2}{2m_2}.$$

6.9.2 Case 2, $n_{\vec{k}\uparrow}=1$, $\varepsilon_{\vec{k}-\vec{q}\downarrow}$:

$$\int_{n_{\vec{k}\uparrow=1},K_+\geq 0} d\vec{k}\delta(\omega+\varepsilon_{\vec{k}-\vec{q}\downarrow}-\varepsilon_{\vec{k}\uparrow}) = M\log\left(\frac{\sqrt{k_{2,+,-}^2+P_+^2}+k_{2,+,-}}{\sqrt{k_{2,-,-}^2+P_+^2}+k_{2,-,-}}\right)+M\log\left(\frac{\sqrt{k_{2,+,+}^2+P_+^2}+k_{2,+,+}}{\sqrt{k_{2,-,+}^2+P_+^2}+k_{2,-,+}}\right),$$

$$\int_{n_{\vec{k}\uparrow}=1,K_+\leq 0} d\vec{k}\ \delta(\omega+\varepsilon_{\vec{k}-\vec{q}\downarrow}-\varepsilon_{\vec{k}\uparrow}) = 2M\log\left(\frac{\sqrt{(k_{2,+}+Y_2)^2-P_+^2}+(k_{2,+}+Y_2)}{\sqrt{(k_{2,-}+Y_2)^2-P_+^2}+(k_{2,-}+Y_2)}\right),$$

$$k_{2,\pm}=\frac{-Y_2(M-R)\pm\sqrt{4K_+M^2(M-R)+8\mu M^2R-Y_2^2(M^2-R^2)}}{2M},$$
$$k_{2,\pm,\pm}=\pm\sqrt{\frac{(M+R)[|Y_2|\,(2Mk_{2,\pm}+Y_2(M-R))-2K_+M^2+Y_2^2R]+4\mu M^2R}{2M^2}},$$

$$\omega_{2,0}=\frac{k_{F,1}^2}{2m_1}-\frac{k_{F,1}^2}{2m_2}-\frac{q_y^2}{2m_2}\left(\frac{m_1m_2}{m_1^2-m_2^2}\right),$$
$$\omega_{2,\pm}=\frac{k_{F,2}^2}{2m_2}-\frac{(k_{F,2}\mp|q_y|)^2}{2m_1}.$$

6.9.3 Case 3, $n_{\vec{k}\downarrow}=1$, $\varepsilon_{\vec{k}+\vec{q}\uparrow}$:

$$\int_{n_{\vec{k}\downarrow}=1,K_+\geq 0} d\vec{k}\delta(\omega+\varepsilon_{\vec{k}\downarrow}-\varepsilon_{\vec{k}+\vec{q}\uparrow}) = M\log\left(\frac{\sqrt{k_{3,+,-}^2+P_+^2}+k_{3,+,-}}{\sqrt{k_{3,-,-}^2+P_+^2}+k_{3,-,-}}\right)+M\log\left(\frac{\sqrt{k_{3,+,+}^2+P_+^2}+k_{3,+,+}}{\sqrt{k_{3,-,+}^2+P_+^2}+k_{3,-,+}}\right),$$

$$\int_{n_{\vec{k}\downarrow}=1,K_+\leq 0} d\vec{k}\delta(\omega+\varepsilon_{\vec{k}\downarrow}-\varepsilon_{\vec{k}+\vec{q}\uparrow}) = 2M\log\left(\frac{\sqrt{(k_{3,+}+Y_1)^2-P_+^2}+(k_{3,+}+Y_1)}{\sqrt{(k_{3,-}+Y_1)^2-P_+^2}+(k_{3,-}+Y_1)}\right),$$

$$k_{3,\pm}=\frac{-Y_1(M+R)\pm\sqrt{4K_+M^2(M+R)+8\mu M^2R-Y_1^2(M^2-R^2)}}{2M},$$
$$k_{3,\pm,\pm}=\pm\sqrt{\frac{(M-R)(|Y_1|[2Mk_{3,\pm}+Y_1(M+R)]-2K_+M^2-RY_1^2)+4\mu RM^2}{2M^2}},$$

$$\omega_{3,0} = \frac{k_{F,2}^2}{2m_1} - \frac{k_{F,2}^2}{2m_2} - \frac{q_y^2}{2m_1}\left(\frac{m_1 m_2}{m_1^2 - m_2^2}\right),$$
$$\omega_{3,\pm} = \frac{\left(k_{F,1} \pm |q_y|\right)^2}{2m_2} - \frac{k_{F,1}^2}{2m_1}.$$

6.9.4 Case 4, $n_{\vec{k}\downarrow} = 1$, $\varepsilon_{\vec{k}-\vec{q}\uparrow}$:

$$\int_{n_{\vec{k}\downarrow}=1, K_- \leq 0} d\vec{k}\delta(\omega + \varepsilon_{\vec{k}-\vec{q}\uparrow} - \varepsilon_{\vec{k}\downarrow})$$
$$= M \log\left(\frac{\sqrt{k_{4,+,-}^2 - P_-^2} + k_{4,+,-}}{\sqrt{k_{4,-,-}^2 - P_-^2} + k_{4,-,-}}\right) + M \log\left(\frac{\sqrt{k_{4,+,+}^2 - P_-^2} + k_{4,+,+}}{\sqrt{k_{4,-,+}^2 - P_-^2} + k_{4,-,+}}\right),$$

$$\int_{n_{\vec{k}\downarrow}=1, K_- \geq 0} d\vec{k}\delta(\omega + \varepsilon_{\vec{k}-\vec{q}\uparrow} - \varepsilon_{\vec{k}\downarrow}) = 2M \log\left(\frac{\sqrt{P_-^2 + (k_{4,+} - Y_1)^2} + (k_{4,+} - Y_1)}{\sqrt{P_-^2 + (k_{4,-} - Y_1)^2} + (k_{4,-} - Y_1)}\right),$$

$$k_{4,\pm} = \frac{Y_1(M+R) \pm \sqrt{-4K_- M^2(M+R) + 8\mu M^2 R - Y_1^2(M^2 - R^2)}}{2M},$$
$$k_{4,\pm,\pm} = \pm\sqrt{\frac{(M-R)(|Y_1|[2Mk_{4,\pm} - Y_1(M+R)] + 2K_- M^2 - RY_1^2) + 4\mu R M^2}{2M^2}},$$

$$\omega_{4,0} = \frac{k_{F,2}^2}{2m_2} - \frac{k_{F,2}^2}{2m_1} + \frac{q_y^2}{2m_1}\left(\frac{m_1 m_2}{m_1^2 - m_2^2}\right),$$
$$\omega_{4,\pm} = \frac{k_{F,1}^2}{2m_1} - \frac{\left(k_{F,1} \mp |q_y|\right)^2}{2m_2}.$$

6.10 Details of computing $\mathrm{Im}\chi^{(0)}_{\hat{S}_z\hat{S}_z}(\vec{q},\omega)$

We wish to compute the imaginary part of the $\chi^{(0)}_{\hat{S}_z\hat{S}_z}(\vec{q},\omega)$ for the dispersion relation modelling the altermagnetic phase. That is, computing

$$\mathrm{Im}\chi^{(0)}_{\hat{S}_z\hat{S}_z}(\vec{q},\omega) = -\frac{\pi}{4(2\pi)^d}\sum_{\sigma}\left[\int_{n_{\vec{k}\sigma}=1} d\vec{k}\delta(\omega+\varepsilon_{\vec{k}\sigma}-\varepsilon_{\vec{k}+\vec{q}\sigma}) - \int_{n_{\vec{k}\sigma}=1} d\vec{k}\delta(\omega+\varepsilon_{\vec{k}-\vec{q}\sigma}-\varepsilon_{\vec{k}\sigma})\right],$$

where

$$\varepsilon(\sigma,\vec{k}) = \delta_{\sigma\uparrow}\left(\frac{k_x^2}{2m_1}+\frac{k_y^2}{2m_2}\right)+\delta_{\sigma\downarrow}\left(\frac{k_y^2}{2m_1}+\frac{k_x^2}{2m_2}\right).$$

Let $f_\sigma(k_x,k_y) = \omega+\varepsilon_{\vec{k}\sigma}-\varepsilon_{\vec{k}+\vec{q}\sigma}$. Then,

$$f_\sigma(k_x,k_y) = -\frac{k_xq_x}{m_i}-\frac{k_yq_y}{m_{\bar{i}}}-\frac{q_x^2}{2m_i}-\frac{q_y^2}{2m_{\bar{i}}}+\omega,$$

where $i=1$ and $\bar{i}=2$ if $\sigma=\uparrow$. Otherwise, if $\sigma=\downarrow$, $i=2$ and $\bar{i}=1$. The curves $\delta(\omega+\varepsilon_{\vec{k}\sigma}-\varepsilon_{\vec{k}+\vec{q}\sigma})$ and $\delta(\omega+\varepsilon_{\vec{k}-\vec{q}\sigma}-\varepsilon_{\vec{k}\sigma})$ are determined by $f_\sigma(k_x,k_y)=0$ and $h_\sigma(k_x,k_y)=0$ respectively.

$$f_\sigma(k_x,k_y)=0 \Rightarrow k_{y,1}(k_x) = -\frac{2k_xm_{\bar{i}}q_x-2m_im_{\bar{i}}\omega+m_iq_y^2+m_{\bar{i}}q_x^2}{2m_iq_y}. \tag{6.5}$$

Eq. (6.5) is linear in k_x, meaning it forms a straight lines in momentum space. Using the Dirac delta decomposition in Eq. (3.2),

$$\begin{aligned}\int_{n_{\vec{k}\sigma}=1} d\vec{k}\delta(\omega+\varepsilon_{\vec{k}\sigma}-\varepsilon_{\vec{k}+\vec{q}\sigma}) &= \frac{m_{\bar{i}}}{|q_y|}\int_{-\sqrt{2m_i\mu}}^{\sqrt{2m_i\mu}}\int_{-\sqrt{2m_{\bar{i}}\mu-\frac{m_{\bar{i}}}{m_i}k_x^2}}^{\sqrt{2m_{\bar{i}}\mu-\frac{m_{\bar{i}}}{m_i}k_x^2}}\delta(k_y-k_{y,1}(k_x))\,dk_ydk_x,\\ &= \frac{m_{\bar{i}}}{|q_y|}\int_{-\sqrt{2m_i\mu}}^{\sqrt{2m_i\mu}}\Theta\left(\mu-\frac{k_x^2}{2m_i}-\frac{k_{y,1}(k_x)^2}{2m_{\bar{i}}}\right)\,dk_x.\end{aligned}$$

Solving for the theta function gives

$$k_{x,\pm} = \frac{1}{2}\left(-q_x+\frac{2m_im_{\bar{i}}q_x\omega}{m_iq_y^2+m_{\bar{i}}q_x^2}\pm\sqrt{\frac{4m_i^2q_y^2(2\mu+\omega)}{m_iq_y^2+m_{\bar{i}}q_x^2}-\frac{4m_i^3m_{\bar{i}}q_y^2\omega^2}{\left(m_iq_y^2+m_{\bar{i}}q_x^2\right)^2}-\frac{m_iq_y^2}{m_{\bar{i}}}}\right).$$

Then, the integral is obtained as

$$\begin{aligned}\int_{n_{\vec{k}\sigma}=1} d\vec{k}\delta(\omega+\varepsilon_{\vec{k}\sigma}-\varepsilon_{\vec{k}+\vec{q}\sigma}) &= \frac{m_{\bar{i}}}{|q_y|}\int_{k_{x,-}}^{k_{x,+}}dk_x,\\ &= \sqrt{\frac{4m_i^2m_{\bar{i}}^2(2\mu+\omega)}{m_iq_y^2+m_{\bar{i}}q_x^2}-\frac{4m_i^3m_{\bar{i}}^3\omega^2}{\left(m_iq_y^2+m_{\bar{i}}q_x^2\right)^2}-m_im_{\bar{i}}}.\end{aligned}$$

In the same way, in computing $\int_{n_{\vec{k}\sigma}=1} d\vec{k}\delta(\omega+\varepsilon_{\vec{k}-\vec{q}\sigma}-\varepsilon_{\vec{k}\sigma})$, we obtain

$$k_{x,\pm}=\frac{1}{2}\left(q_x+\frac{2m_im_{\bar{i}}q_x\omega}{m_iq_y^2+m_{\bar{i}}q_x^2}\pm\sqrt{\frac{4m_i^2q_y^2(2\mu-\omega)}{m_iq_y^2+m_{\bar{i}}q_x^2}-\frac{4m_i^3m_{\bar{i}}q_y^2\omega^2}{\left(m_iq_y^2+m_{\bar{i}}q_x^2\right)^2}-\frac{m_iq_y^2}{m_{\bar{i}}}}\right).$$

Then, the integral is given by

$$\begin{aligned}\int_{n_{\vec{k}\sigma}=1} d\vec{k}\delta(\omega+\varepsilon_{\vec{k}-\vec{q}\sigma}-\varepsilon_{\vec{k}\sigma}) &= \frac{m_{\bar{i}}}{|q_y|}\int_{k_{x,-}}^{k_{x,+}} dk_x,\\ &= \sqrt{\frac{4m_i^2m_{\bar{i}}^2(2\mu-\omega)}{m_iq_y^2+m_{\bar{i}}q_x^2}-\frac{4m_i^3m_{\bar{i}}^3\omega^2}{\left(m_iq_y^2+m_{\bar{i}}q_x^2\right)^2}-m_im_{\bar{i}}}.\end{aligned}$$

Then, the susceptibility is given by

$$\begin{aligned}\mathrm{Im}\chi^{(0)}_{\hat{S}_z\hat{S}_z}(\vec{q},\omega) = -\frac{\pi}{4(2\pi)^d}\sum_\sigma\Bigg[&\sqrt{\frac{4m_i^2m_{\bar{i}}^2(2\mu+\omega)}{m_iq_y^2+m_{\bar{i}}q_x^2}-\frac{4m_i^3m_{\bar{i}}^3\omega^2}{\left(m_iq_y^2+m_{\bar{i}}q_x^2\right)^2}-m_im_{\bar{i}}}\\ &-\sqrt{\frac{4m_i^2m_{\bar{i}}^2(2\mu-\omega)}{m_iq_y^2+m_{\bar{i}}q_x^2}-\frac{4m_i^3m_{\bar{i}}^3\omega^2}{\left(m_iq_y^2+m_{\bar{i}}q_x^2\right)^2}-m_im_{\bar{i}}}\Bigg].\end{aligned}$$

Lines determining non-analytic features and limiting or special excitation processes are given by

$$\begin{aligned}\omega_{\sigma,-,\pm} &= \pm\sqrt{\frac{2\mu q_x^2}{m_i}+\frac{2\mu q_y^2}{m_{\bar{i}}}}-\frac{q_x^2}{2m_i}-\frac{q_y^2}{2m_{\bar{i}}}\\ \omega_{\sigma,+,\pm} &= \pm\sqrt{\frac{2\mu q_x^2}{m_i}+\frac{2\mu q_y^2}{m_{\bar{i}}}}+\frac{q_x^2}{2m_i}+\frac{q_y^2}{2m_{\bar{i}}}.\end{aligned}$$

6.11 Dissipation of the resonance mode in spin-flip susceptibility $\chi^{(0)}_{+-}(\vec{q},\omega)$

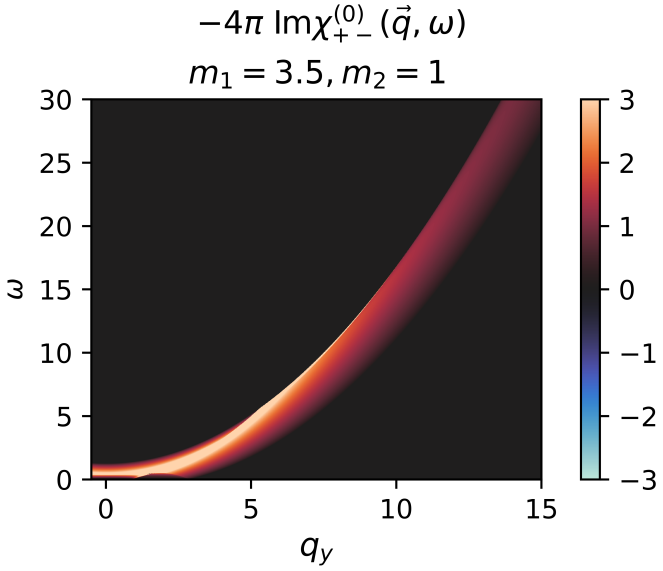

Figure 13: Imaginary part of $\chi^{(0)}_{+-}(\vec{q},\omega)$, displayed for effective electron masses $m_1 = 3.5, m_2 = 1$, corresponding to an enlarged view of the middle panel in Fig.10. The resonance mode, $\omega_{1,+}$ is showed to dissipate at sufficiently large values of q_y and ω, where it converges to $\omega_{1,0}$.

6.12 Longitudinal spin susceptibility results

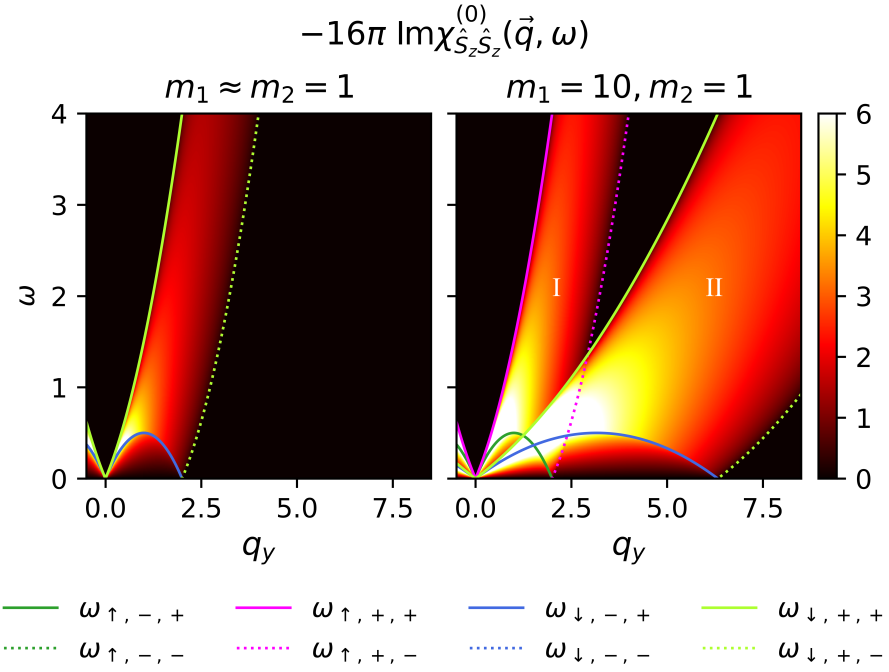

Figure 14: Imaginary part of $\chi^{(0)}_{\hat{S}_z\hat{S}_z}(\vec{q},\omega)$, displayed for different pairs of effective electron masses. The spectrum is symmetric with respect to q_y, and anti-symmetric with respect to ω. Explicit expressions for quantities involved in the plotting are given in Sec. 6.10.

The longitudinal spin susceptibility is displayed in Fig.- 14. Notably, there is not a continuum of allowed excitations at $q_y = 0$ in the altermagnetic case. This is because the excitation processes contributing to this susceptibility do not include the flipping of electron spins, as is mathematically stated in Eq. (2.17). That is, the excitation spectrum only involves electron-hole excitations. Hence, the excitation spectrum is closely related to that in the non-altermagnetic limit, discussed in Sec. 4.1. Furthermore, two branches appear for $q_y \geq 0$ and $\omega \geq 0$ for the altermagnetic phase, reflecting that electrons belong to distinct branches depending on their spins. Increasing m_1 increases the Fermi wave vector $k_{F,1}$, which introduces more states to participate in excitation processes. This results in broadening of the excitation spectrum. As we only consider momenta transfer of form $\vec{q} = (0, q_y)$, broadening will occur for only one branch, as described by the expressions for $\omega_{\sigma,-,\pm}$ and $\omega_{\sigma,+,\pm}$ provided in Sec. 6.10.

Furthermore, by only considering momentum transfer $\vec{q} = (0, q_y)$, we can characterize the Fermi surface associated with each branch. Specifically, the minimum excitation energy of a branch is non-zero when $\vec{k}+\vec{q}$, for $\vec{q} = (0, q_y)$, is guaranteed to be outside of the Fermi surface for any $\vec{k}$ inside of the Fermi surface. This allows us to characterize the branch labelled II in Fig. 14 as being associated with the Fermi surface with its major axis along k_y ($n_{\vec{k}\downarrow} = 1$), to reflect that large q_y values are needed to ensure all electrons will land outside of the Fermi

surface upon excitation.

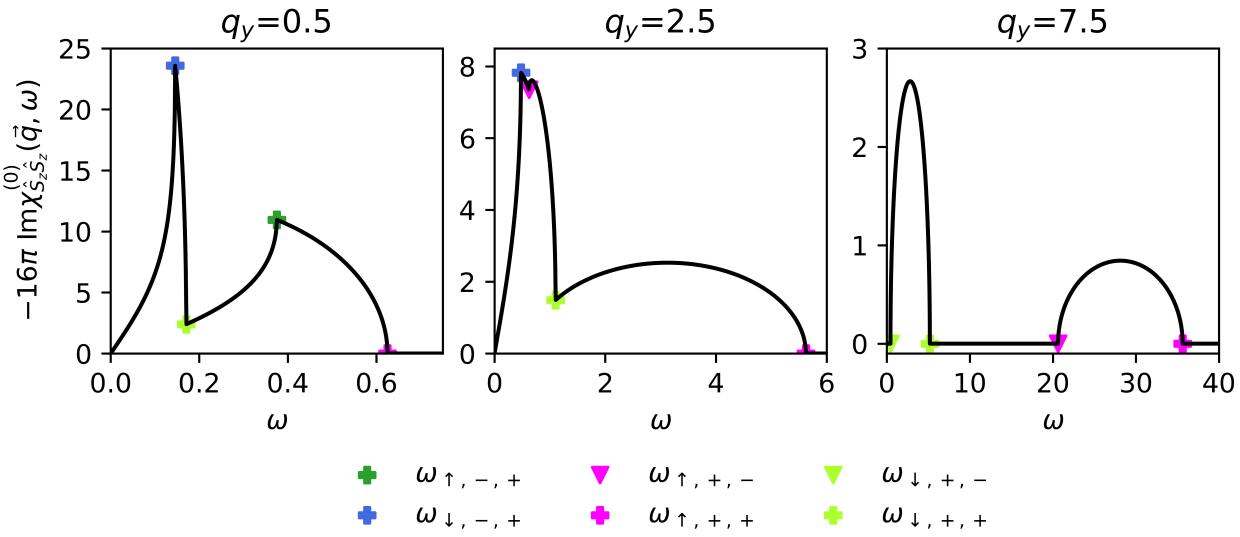

Figure 15: Cross sections taken from the imaginary part of $\chi^{(0)}_{\hat{S}_z\hat{S}_z}(\vec{q},\omega)$ for fixed values of q_y. Here, $m_1 = 10$ and $m_2 = 1$.

The cross sections of the longitudinal spin susceptibility, displayed in Fig. 15, show similar shapes to those observed in the cross sections for the non-altermagnetic limit (Fig. 9). This is a consequence of the nature of the excitation processes being the same (electron-hole excitation without flipping spins). The shapes have different widths due to the Fermi surfaces having different lengths of the Fermi wave vectors along the k_y-axis.